AD-A222 229

DTIC COPY

# NAVAL POSTGRADUATE SCHOOL
## Monterey, California

# THESIS

DTIC
ELECTE
JUN 0 4 1990
S D
Cc E

UNDERWATER SOUND RADIATED BY IMPACTS AND BUBBLES CREATED BY RAINDROPS

by

Armagan Kurgan

December 1989

Thesis Advisor — Herman Medwin
Co-Advisor — Jeffrey A. Nystuen

Approved for public release; distribution is unlimited.

## REPORT DOCUMENTATION PAGE

| | | | |
|---|---|---|---|
| 1a Report Security Classification Unclassified | | | 1b Restrictive Markings |
| 2a Security Classification Authority | | | 3 Distribution Availability of Report |
| 2b Declassification Downgrading Schedule | | | Approved for public release; distribution is unlimited. |
| 4 Performing Organization Report Number(s) | | | 5 Monitoring Organization Report Number(s) |
| 6a Name of Performing Organization<br>Naval Postgraduate School | 6b Office Symbol<br>*(if applicable)* 33 | | 7a Name of Monitoring Organization<br>Naval Postgraduate School |
| 6c Address *(city, state, and ZIP code)*<br>Monterey, CA 93943-5000 | | | 7b Address *(city, state, and ZIP code)*<br>Monterey, CA 93943-5000 |
| 8a Name of Funding Sponsoring Organization | 8b Office Symbol<br>*(if applicable)* | | 9 Procurement Instrument Identification Number |
| 8c Address *(city, state, and ZIP code)* | | | 10 Source of Funding Numbers |
| | | | Program Element No / Project No / Task No / Work Unit Accession No |

11 Title *(include security classification)* UNDERWATER SOUND RADIATED BY IMPACTS AND BUBBLES CREATED BY RAINDROPS

12 Personal Author(s) Armagan Kurgan

| 13a Type of Report | 13b Time Covered | 14 Date of Report *(year, month, day)* | 15 Page Count |
|---|---|---|---|
| Master's Thesis | From To | December 1989 | 76 |

16 Supplementary Notation The views expressed in this thesis are those of the author and do not reflect the official policy or position of the Department of Defense or the U.S. Government.

| 17 Cosati Codes | | | 18 Subject Terms *(continue on reverse if necessary and identify by block number)* |
|---|---|---|---|
| Field | Group | Subgroup | Raindrops, impacts, bubbles, energy, radiation pattern, Thesis |
| | | | |
| | | | |

19 Abstract *(continue on reverse if necessary and identify by block number)*

The sound generated by rainfall at sea is caused by raindrops of a wide range of sizes and angles of incidence, which fall at their terminal velocities. The purpose of this laboratory research has been to make complete acoustical measurements of the sound generated by single water drops striking the water surface at their terminal velocities for normal and oblique incidence. This has included the total acoustic energy, peak axial pressure, frequency spectrum and polar radiation pattern.

Depending on the drop size and the angle of incidence, many drops falling at their terminal velocities create bubbles. At all angles of incidence studied here the sound radiated by an individual bubble contains more energy than the sound from an individual impact.

These results, using terminal velocities and oblique trajectories, are very different from the published normal incidence, non-terminal velocity characterizations. For example bubble frequencies other than the well known 14 kHz peak are found. Also the energy of the impact sound increases significantly for larger drop sizes and for larger deviations from normal trajectories. Furthermore, drops of diameter 0.8 mm to 1 mm, which always produce bubles at normal incidence, create bubbles only about 10 % of the impacts at oblique incidence. These observations provide specific reasons for the previously unexplained broadening, shifting and reduction in magnitude of the 14 kHz spectral peak of the rain noise in the presence of winds at sea.

| 20 Distribution Availability of Abstract | 21 Abstract Security Classification | |
|---|---|---|
| ☒ unclassified unlimited ☐ same as report ☐ DTIC users | Unclassified | |
| 22a Name of Responsible Individual<br>Herman Medwin | 22b Telephone *(include Area code)*<br>(408) 646-2385 | 22c Office Symbol<br>61MD |

DD FORM 1473,84 MAR 83 APR edition may be used until exhausted
All other editions are obsolete

Approved for public release; distribution is unlimited.

Underwater sound radiated by
impacts and bubbles created by raindrops

by

Armagan Kurgan
LTJG, Turkish Navy
B.S., Naval Academy, Istanbul, 1983

Submitted in partial fulfillment of the
requirements for the degree of

MASTER OF SCIENCE IN ENGINEERING ACOUSTICS

from the

NAVAL POSTGRADUATE SCHOOL
December 1989

Author: _____
Armagan Kurgan

Approved by: _____
Herman Medwin, Thesis Advisor

_____
Jeffrey A. Nystuen, Co-Advisor

_____
Anthony A. Atchley, Chairman,
Engineering Acoustics Academic Comittee

## ABSTRACT

The sound generated by rainfall at sea is caused by raindrops of a wide range of sizes and angles of incidence, which fall at their terminal velocities. The purpose of this laboratory research has been to make complete acoustical measurements of the sound generated by single water drops striking the water surface at their terminal velocities for normal and oblique incidence. These measurements have included the total acoustic energy, peak axial pressure, frequency spectrum and polar radiation pattern.

Depending on the drop size and the angle of incidence, many drops falling at their terminal velocities create bubbles. At all angles of incidence studied here the sound radiated by an individual bubble contains more energy than the sound from an individual impact.

These results, using terminal velocities and oblique trajectories, are very different from the published normal incidence, non-terminal velocity characterizations. For example bubble frequencies other than the well known 14 kHz peak are found. Also the energy of the impact sound increases significantly for larger drop sizes and for larger deviations from normal trajectories. Furthermore, drops of diameter 0.8 mm to 1 mm, which always produce bubbles at normal incidence, create bubbles only about 10 % of the impacts at oblique incidence. These observations provide specific reasons for the previously unexplained broadening, shifting and reduction in magnitude of the 14 kHz spectral peak of the rain noise in the presence of winds at sea.


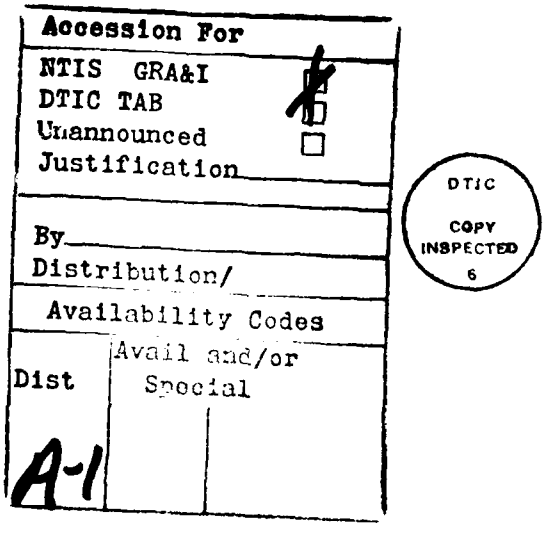

## TABLE OF CONTENTS


I. INTRODUCTION . . . . . 1

II. THEORY OF THE EXPERIMENT . . . . . 5

III. EXPERIMENT . . . . . 7
A. EQUIPMENT . . . . . 7
1. Mechanical . . . . . 7
2. Optical . . . . . 7
3. Acoustical . . . . . 7
4. Electronic . . . . . 8
5. Experimental Procedure . . . . . 8
B. NORMAL INCIDENCE . . . . . 10
1. Peak Axial Pressure . . . . . 12
2. Total Acoustic Energy . . . . . 20
3. Frequency Specta . . . . . 26
4. Radiation Pattern . . . . . 30
C. OBLIQUE INCIDENCE . . . . . 34
1. Peak Axial Pressure . . . . . 34
2. Total Acoustic Energy . . . . . 37
3. Frequency Spectra . . . . . 46
4. Percentage of Drops Creating Bubbles . . . . . 53
5. Radiation Pattern . . . . . 56

IV. CONCLUSIONS . . . . . 59

APPENDIX A. PREAMPLIFIER 1 . . . . . 61

APPENDIX B. PREAMPLIFIER 2 . . . . . 62

LIST OF REFERENCES . . . . . 63

INITIAL DISTRIBUTION LIST ..... 64

## LIST OF FIGURES


Figure 1. Noise at sea . . . . . 2
Figure 2. Regions of regular and random bubble creation . . . . . 3
Figure 3. Experimental setup . . . . . 9
Figure 4. Bubble creation region including small drops . . . . . 11
Figure 5. Acoustic pressure of an impact and a bubble. . . . . 13
Figure 6. Acoustic pressure caused by impact . . . . . 14
Figure 7. Acoustic pressure caused by bubble . . . . . 15
Figure 8. Average peak axial pressures for impacts . . . . . 16
Figure 9. Average peak axial pressures for bubbles . . . . . 17
Figure 10. Peak axial pressure histograms of impacts . . . . . 18
Figure 11. Peak axial pressure histograms of bubbles . . . . . 19
Figure 12. Average acoustic energies radiated by the impacts . . . . . 22
Figure 13. Average acoustic energies radiated by the bubbles . . . . . 23
Figure 14. Acoustic energy histograms of the impacts . . . . . 24
Figure 15. Acoustic energy histograms of the bubbles . . . . . 25
Figure 16. Frequency spectrum of the impact sound. . . . . 27
Figure 17. Peak frequencies of impacts . . . . . 28
Figure 18. Resonance frequencies of bubbles . . . . . 29
Figure 19. Eight hydrophone array with 20 degere separations . . . . . 31
Figure 20. Eight hydrophone array with 10 degree separations . . . . . 32
Figure 21. Polar radiation pattern of normal incidence drops . . . . . 33
Figure 22. Average peak axial pressures for impacts . . . . . 35
Figure 23. Average peak axial pressures for bubbles . . . . . 36
Figure 24. Max. min. and avg. impact acoustic energies for 0.83 mm drops . . . . . 38
Figure 25. Max. min. and avg. impact acoustic energies for 0.914 mm drops . . . . . 39
Figure 26. Max. min. and avg. impact acoustic energies for 0.985 mm drops . . . . . 40
Figure 27. Average impact acoustic energies of the drops . . . . . 41
Figure 28. Radiated bubble energy for 0.83 mm drops . . . . . 42
Figure 29. Radiated bubble energy for 0.914 mm drops . . . . . 43
Figure 30. Radiated bubble energy for 0.985 mm drops . . . . . 44
Figure 31. Average bubble acoustic energies for oblique incidence . . . . . 45

Figure 32. Frequency spectrum of an impact sound ..... 47
Figure 33. Avg. peak frequencies of impact sound for oblique inc. drops ..... 48
Figure 34. Max. min. and avg. resonance frequencies of bubbles for 0.83 mm .... 49
Figure 35. Max. min. and avg. resonance frequencies of bubbles for 0.914 mm ... 50
Figure 36. Max. min. and avg. resonance frequencies of bubbles for 0.985 mm ... 51
Figure 37. Avg. resonance frequencies of bubbles for oblique incidence drops .... 52
Figure 38. Percentage of drops that create bubbles ..... 54
Figure 39. The ratio of the average bubble energy to the impact energy ..... 55
Figure 40. Polar radiation pattern of bubbles for 10 degrees incidence ..... 57
Figure 41. Polar radiation pattern of bubbles for 20 degrees incidence ..... 58

## LIST OF SYMBOLS AND ABBREVIATIONS

| SYMBOL | UNITS | NAME / DESCRIPTION |
|---|---|---|
| $\rho$ | kg/ m$^3$ | Water density |
| c | m/ sec | Speed of sound in water |
| w | m/ sec | Particle velocity |
| R | meter | Range of hydrophone on the axis |
| p | pascals | Pressure |
| k | radians/ meters | Acoustic wave number |
| KE | Joules | Kinetic energy |
| m | kg | Mass |
| $\theta$ | degrees | Angle from the vertical acoustic axis |
| v | meters/ sec | Velocity |

## ACKNOWLEDGEMENTS

I wish to express my sincere appreciation to Professor Herman Medwin of the Physics department, U.S Naval Postgraduate School, for his guidance, encouragement and patience which made this study a great learning experience; to Professor Jeffrey A. Nystuen for his invaluable help in all parts of the experiment, to LTJG Olmez for spending his summer vacation in my laboratory, trying hard for video film of the drops and to my wife Fazilet for her support, understanding and love.

# I. INTRODUCTION

There have been no theoretical studies of the sound generated by rainfall at oblique incidence, which most probably always occurs because of the wind as well as the roughness of the sea surface. Instead there have been theoretical studies (Franz, 1959), (Longuet-Higgins, 1989), (Oguz and Prosperetti, 1989) for normal incidence. Also there have been no experimental results published before for oblique incidence of single drops. Instead there have been several experiments for drops at normal and non-terminal velocities. The purpose of this thesis is to study the sound generated by raindrops striking the water surface at oblique incidence and at normal incidence.

Several previous experiments, both with natural and artificial rain, have verified that the main feature of the noise spectrum generated by rain at sea is a peak at about 14 kHz. (Nystuen and Farmer, 1987). This peak broadens, shifts to higher frequencies and decreases in magnitude as the wind speed increases (Figure 1).

G.J.Franz (1959) concluded a laboratory study of single drops by asserting that rain drops create noise by two different mechanisms: IMPACT and OSCILLATION of the bubbles created by the drops. He also concluded that at low impact velocities bubble noise dominates but at high impact velocities bubbles are less likely to be formed so that the sound generated by a raindrop at its terminal velocity could be considered as the sound from the impact only.

Later studies showed that oscillating air bubbles are more important noise sources than Franz had argued. Pumphrey and Crum (1989) conducted experiments for normally incident single drops with different sizes and different impact velocities as shown in Figure 2. Their explanation follows : the shaded area is a region of consistent bubble creation. In the range below this region the impact is not energetic enough to create a bubble. Above the region the energy is excessive. At still higher velocities and drop sizes (upper right corner) there is another region for which bubbles occur in an irregular and random fashion. The curve at the left of Figure 2 shows the terminal velocity of drops as a function drop diameter. The range of drop diameters where this terminal velocity curve intersects the shaded region and causes bubble entrainment is the narrow region, stated by them as

$$0.8 \text{ mm} < \text{DROP DIAMETER} < 1.1 \text{ mm}$$

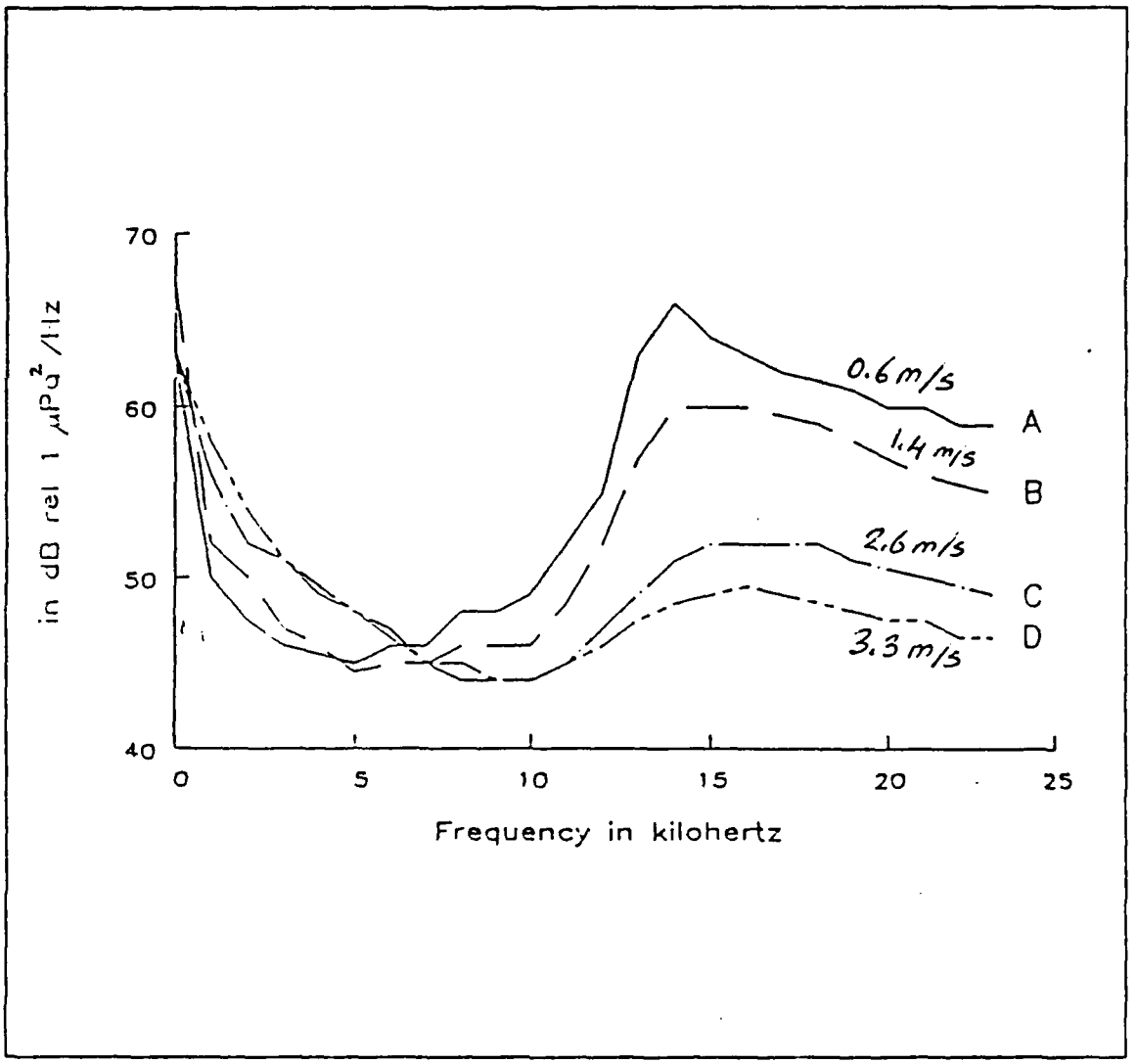


**Figure 1. Noise at sea:** This figure is taken from Nystuen and Farmer (1987). It shows the noise spectra at sea for different wind conditions.

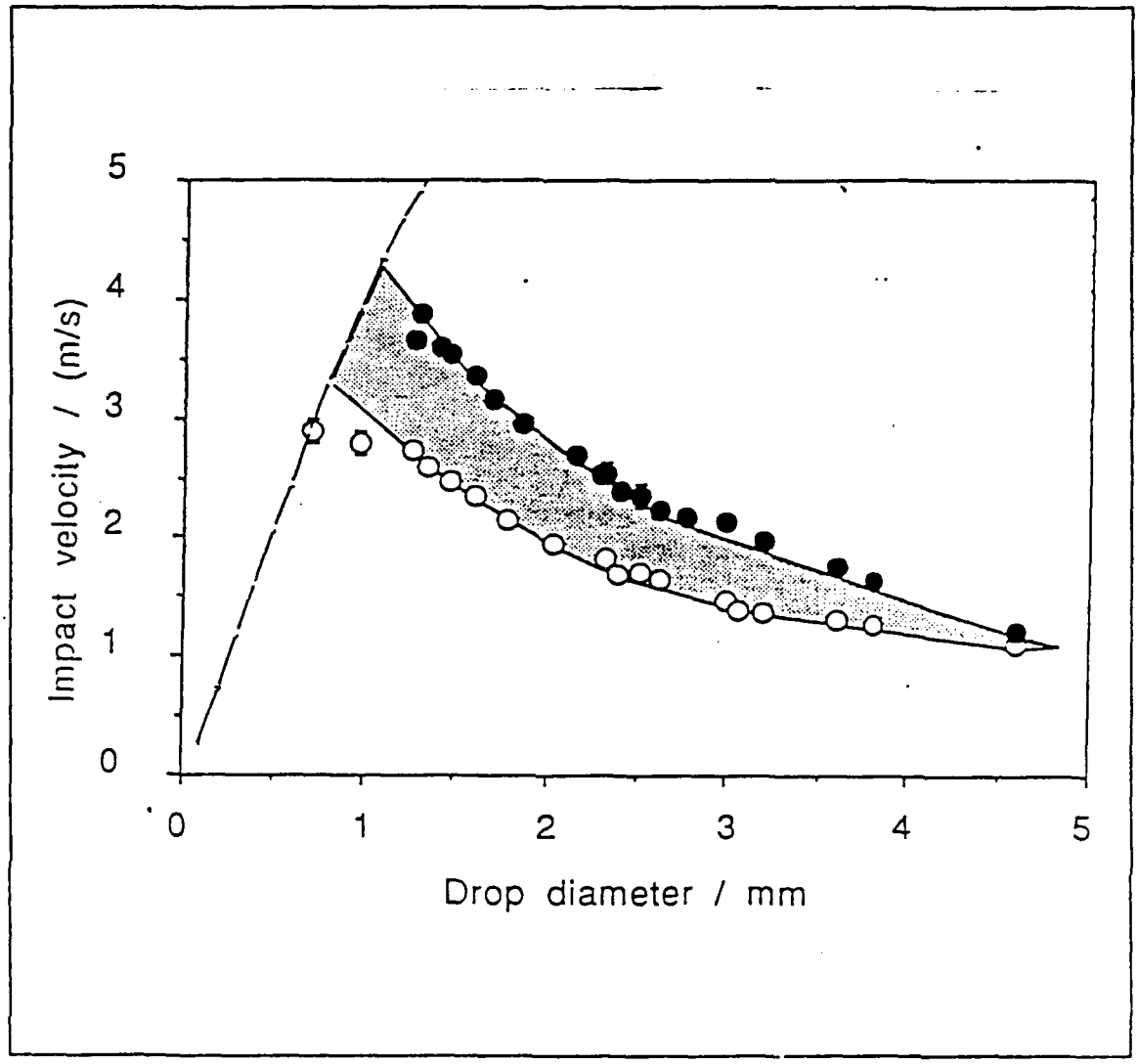


**Figure 2. Regions of regular and random bubble creation:** This figure is taken from Crum and Pumphrey (1989). The shaded area shows the regular bubble creation area and the upper right corner is the irregular (random) bubble creation area.

Crum and Pumphrey argue that the bubbles entrained by these drops have narrowly defined sizes and that they oscillate at a frequency around 14.5 kHz. Only drops in this range entrain bubbles with high probability. Since bubble sound is louder and in a narrower frequency band than the impact sound, they conclude that these particular drops lead to the formation of the 14 kHz peak in rainfall. Furthermore, since drops of this bubble-producing size are likely present in both natural and artificial rain they conclude that, even though a small fraction of all drops are capable of creating bubbles, the acoustical effect of this range of drops is dominant.

In this thesis previous experimental results for normal incidence are first verified for small drop sizes which strike the water surface at their terminal velocities. Then acoustical radiation from single water drops striking the water surface at terminal velocity and oblique incidence is studied.

## II. THEORY OF THE EXPERIMENT

Since the radiation pattern of the noise from the bubble as well as the impact noise is assumed to be dipole radiation for both normal and oblique incidence we can find the total acoustic energy produced by knowing the axial pressure. Assuming $p_{ax}(t)$ is the measured acoustic pressure on the axis of the dipole at range R, $p_1$ is the pressure at 1 meter, $p_{1ax}$ is the acoustic pressure on the axis at 1 meter. For a dipole source $p_1 = p_{1ax}\cos\theta$ , where $\theta$ is the angle from the axis. So the acoustic energy can be written as :

$$Energy = \int\int_s (INTENSITY) dS dt$$

$$Energy = \int\int_s p_1 w_1 dS dt$$

where $w_1$ is the particle velocity and dS is the element of area.

When kR > 3 we can use $w_1 = \frac{p_1}{\rho c}$ with less than 10 % error in magnitude, where $\rho$ is the density of the water, c is the speed of sound in the water and k is the acoustic wave number. Doing the area integration by using the ring element $(2\pi R\sin\theta)Rd\theta$ we can find that

$$\frac{Energy}{Time} = (2\pi\frac{R^2}{\rho c})\int_0^{\frac{\pi}{2}} p_{1ax}^2\cos^2\theta\sin\theta d\theta$$

$$= (2\frac{\pi}{3\rho c})R^2 p_{1ax}^2$$

Because the impact sound and the bubble sound are not continuous, it is convenient to do the integration over time by a summation for elements of time in the digitized form.

$$Energy = (2\pi\frac{R^2}{3\rho c})\sum p_{1ax}^2 t$$

This can be compared with the kinetic energy of the rain drop just before the impact time where

$$KE = \frac{1}{2} mv^2$$

# III. EXPERIMENT

## A. EQUIPMENT

### 1. Mechanical

An Eppendorf digital pipette which can produce accurately metered drops from 0.1 $\mu$ liter to 10 $\mu$ liter (0.58 mm to 2.67 mm diameter) was used to create definite sizes of artificial raindrops. The dropper was placed on a plate located at a fixed position of 1.8 meter over the water surface to make sure that all drops strike at the same point over the axial hydrophone. At this height all drops smaller than 0.985 mm diameter reach their terminal velocities (Wang and Pruppacher, 1977). The hydrophones were placed in an anechoic water tank 10 ft x 10 ft x 9.5 ft deep with redwood wedge absorbers.

Oblique incidence was obtained by using a fan to blow the drop horizontally, immediate after it started to fall. The water surface was not disturbed by the wind.

### 2. Optical

To observe the angle of incidence for the oblique incidence case a video camera with 7 lux light requirement and high speed shutter was used together with an HQ video player. The player (Hitachi VT 498 EM) had adjustible time, frame by frame slow motion and view freezing capability which made possible both drop velocity measurements as well as incidence angle.

Alternatively a camera (Canon AE-1) was also used together with an adjustable frequency stroboscope to observe both the impact velocity and the incidence angle of the drops. For both techniques we used a 5 cm x 5 cm string grid behind the paths of the drops to locate the position of the drop.

### 3. Acoustical

An ITC 6050 C hydrophone with high sensitivity (-163 dB ref 1V per $\mu$ Pa) and flat frequency response from 1 to 40 kHz was used to observe the impact and bubble noise for the normal incidence case. For oblique incidence a nine hydrophone array was used. These hydrophones were either LC10 of sensitivity -198 dB or our own hydrophones constructed of 6 mm diameter cylindrical lead zirconate elements. The sensitivities of our own hydrophones are -205 dB. The array was mounted on a 1 8 inch diameter thin semi-circular rod bent to 30 centimeter radius. The hydrophones were

placed every 10 or 20 degrees along the rod. The hydrophones were calibrated by absolute reciprocity and by inter-comparison, using a ping or the impulse from a reference raindrop.

## 4. Electronic

To investigate the polar radiation pattern, nine hydrophones, nine preamplifiers, nine high pass filters, were the input to an IBM PC -XT computer with an RC-Electronics analog to digital converter board. A software package, called COMPUTERSCOPE, having a maximum A/D conversion rate of $10^6$ samples per second and 12 bit amplitude resolution processed the signals. We made our own preamplifiers as shown in Appendices 1 and 2.

Also to calibrate the hydrophones, an HP-4192 Impedance Analyzer, a signal generator, a power amplifier and a transducer were used. The transducer was placed in the far field and was driven with pulsed signals to prevent scattering from the tank walls.

## 5. Experimental Procedure

The experimental setup was as shown in Figure 3. The noise created by the bubble and the impact was recorded by the hydrophone at depth of 1 m, directly below the point of impact for normal incidence and at depth of 20 cm for oblique incidence and for radiation pattern observations. The output of the hydrophone was amplified and passed through a high pass filter. After filtering all the noise below 8 kHz the signal was sent to an IBM PC-XT Computer which had an RC Electronics analog to digital converter board with sixteen input channels.This system made it possible to observe the outputs of several different hydrophones, trigger with a desired voltage level, find out the frequency spectrum, maximum pressures, total energies and radiation patterns of both the bubble and the impact when used with the software package called Computerscope.

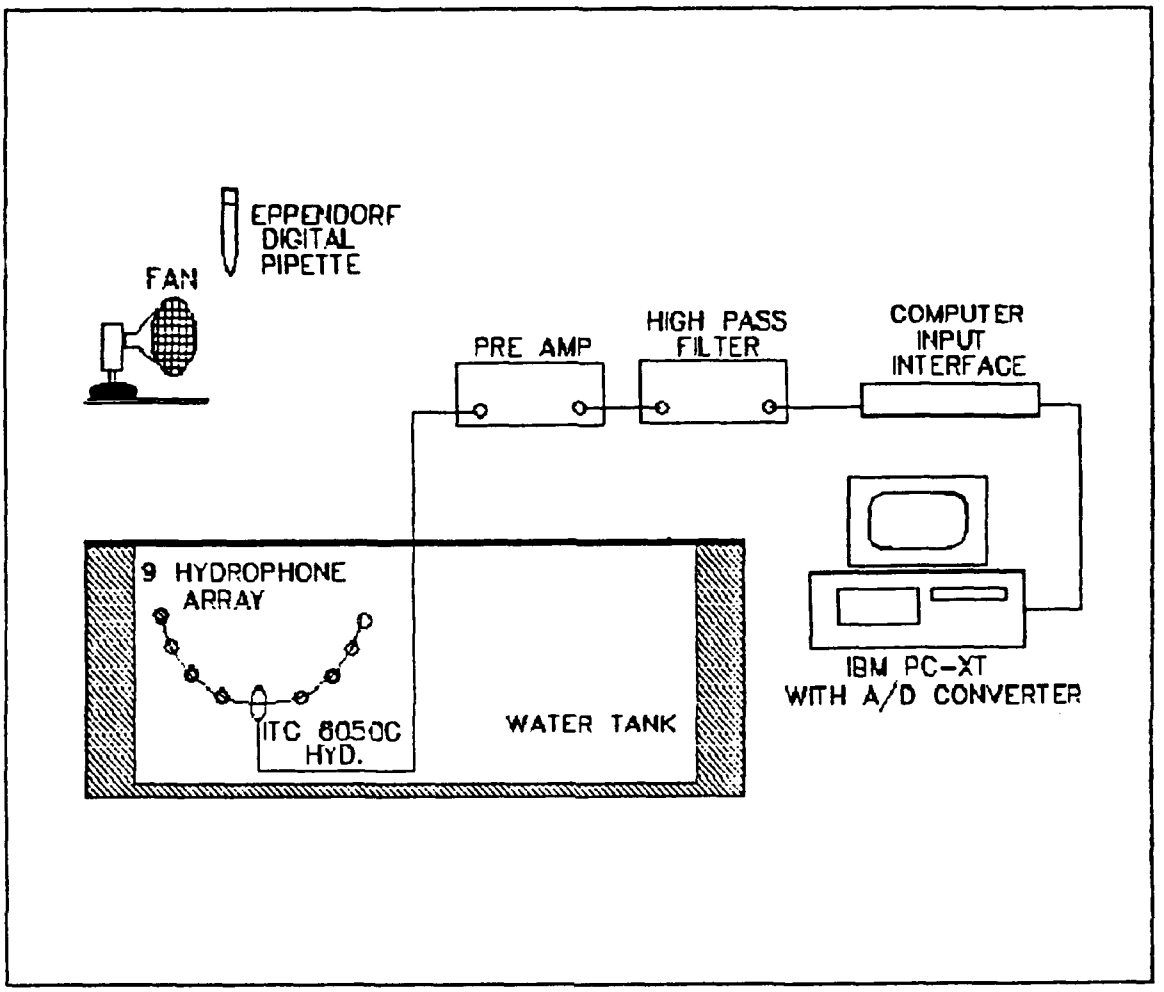


**Figure 3. Experimental setup**

## B. NORMAL INCIDENCE

Initially, different sizes of drops between 0.3 $\mu$ l (0.83mm) to 0.5 $\mu$ l (0.985 mm diameter) that fell normally incident to the tank were used. The fraction of drops that created bubbles was noted for all different drop sizes to compare with the experimental results of Crum and Pumphrey (1989) which is shown in Figure 2. The bubble creation region curve was re-plotted including our data points for near terminal velocities as shown in Figure 4. Our data agreed with theirs, i.e., 98% of the drops created bubbles.

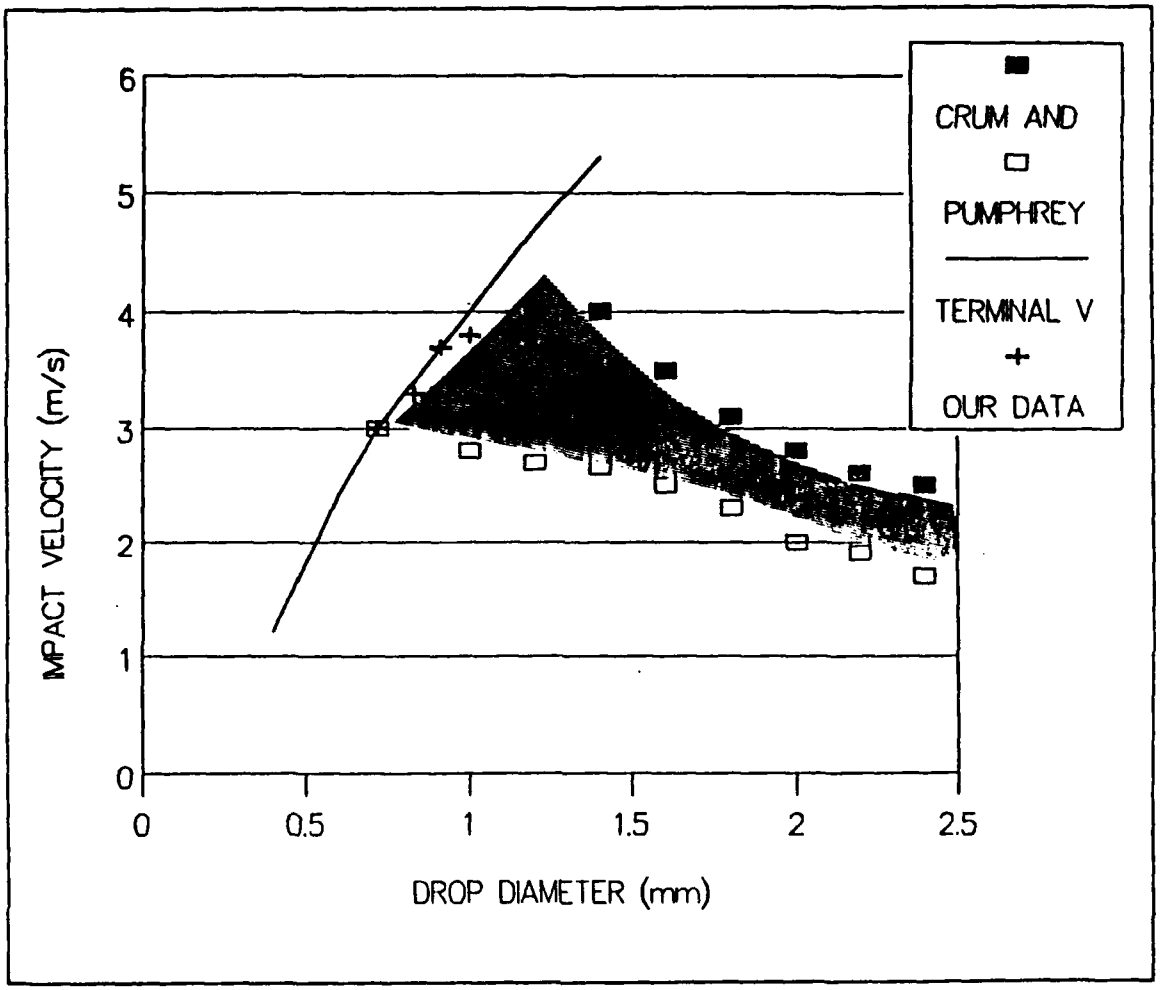


**Figure 4. Bubble creation region including small drops:** This figure is a replot of Figure 2 including our data points, indicated by symbol x, at the terminal velocity curve.

### 1. Peak Axial Pressure

The noise generated by a typical impact is shown in Figure 5 with the bubble noise created by the same drop 17.7 ms after the impact. The same impact and bubble radiation are shown in Figures 6 and 7, with different scales to see the details. As we can see from Figure 5, the peak axial pressure of the bubble is much greater than the peak axial pressure of the impact. For the impact in Figure 6 the peak axial pressure is 460 milivolt after 40 dB amplification The sensitivity of the hydrophone is -163 dB ref 1V per $\mu$ pascal and it is located 20 cm under the water surface. So the calculation of the peak axial pressure is as follows :

$$-163 = 20 \log_{10} \frac{X}{X_{ref}}$$

Since $X_{ref}$ is 1 V per $\mu$ pa, we can write

$$\frac{-163}{20} = \log_{10} X$$

ref 1V per $\mu$ Pa

$$X = 7.08 \times 10^{-9}$$

V per $\mu$ Pa

$$\frac{1}{X} = 141 \times 10^{6} \frac{\mu Pa}{V}$$

$$= 141 \frac{Pa}{volt}$$

The voltage output is 460 mV after 100 times amplification for the hydrophone is on the axis and 20 cm away from the point of impact. So the voltage at the hydrophone for 20 cm is 4.6 mV and for 1 m is 920 $\mu$ V. To find the axial pressure at 1 meter we must simply multiply this value by $\frac{1}{X}$. The result for this particular case is 0.13 pascal. The calculation of the peak axial pressure for the bubbles is the same as for the impacts.

The peak axial pressure for the bubbles and the impacts of different sizes of drops were measured.The average values with standard deviations, and maximum and minimum pressures for different sizes of drops are shown in Figures 8 and 9. The histograms of peak axial pressures for impacts and bubbles are shown in Figures 10 and 11.

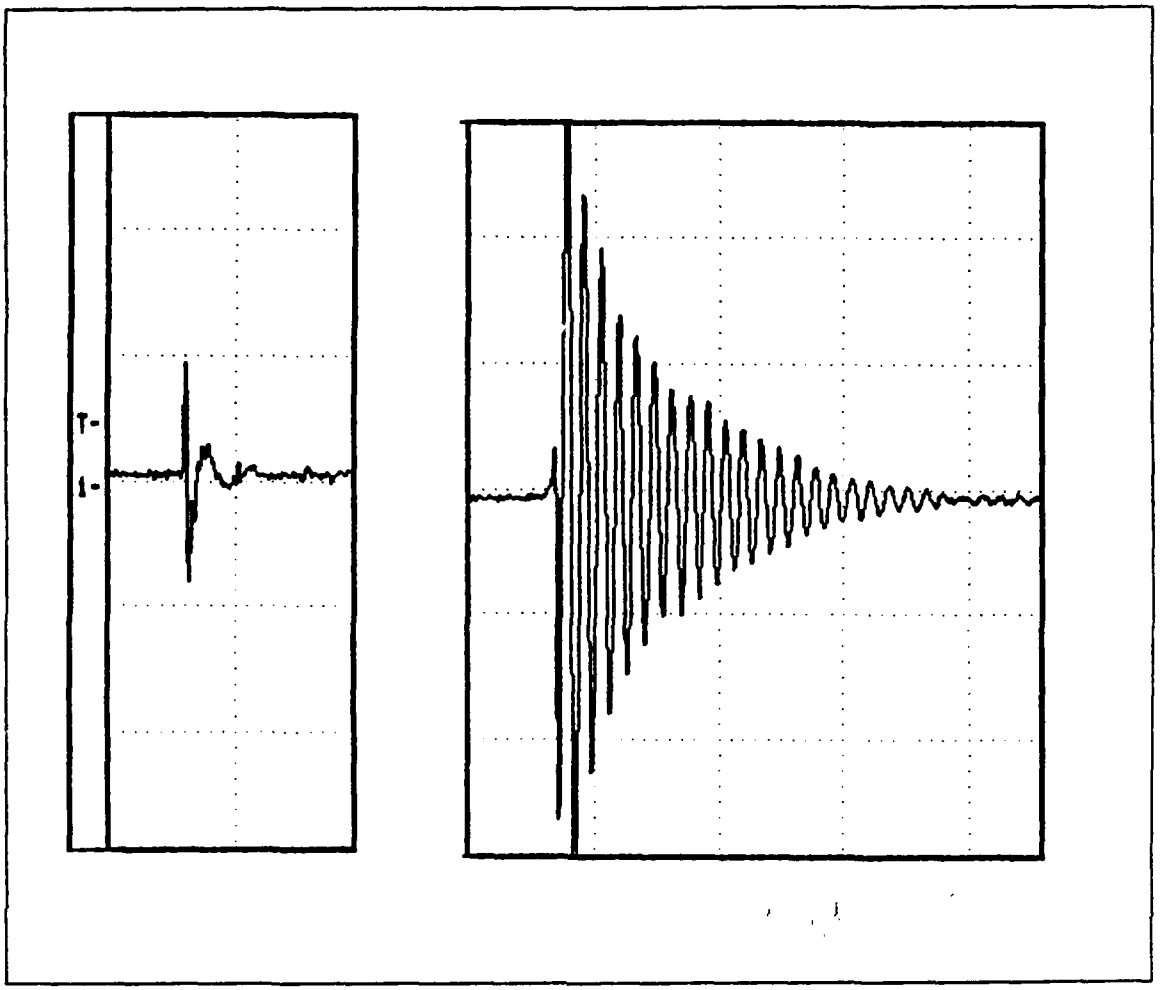

**Figure 5. Acoustic pressure of an impact and a bubble.:** Impact and bubble sound of a 0.83 mm diameter drop. The drop is falling at its terminal velocity, perpendicular to the surface. The time between vertical grid markers is 400 microseconds.

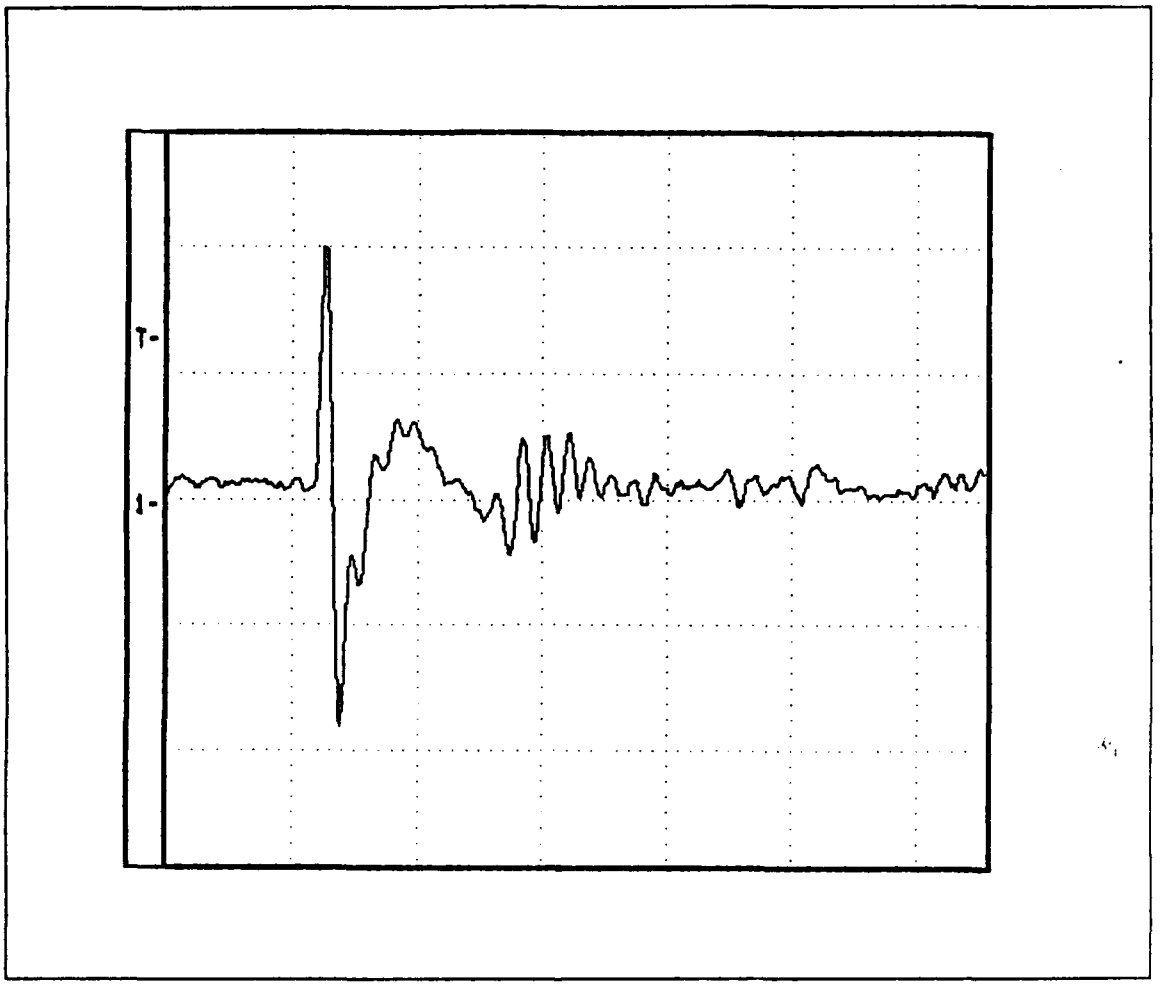


**Figure 6. Acoustic pressure caused by impact:** The same impact shown in Figure 5, with 100 microseconds between vertical grid lines and the amplitude increased by a factor of 2.5 to see the details.

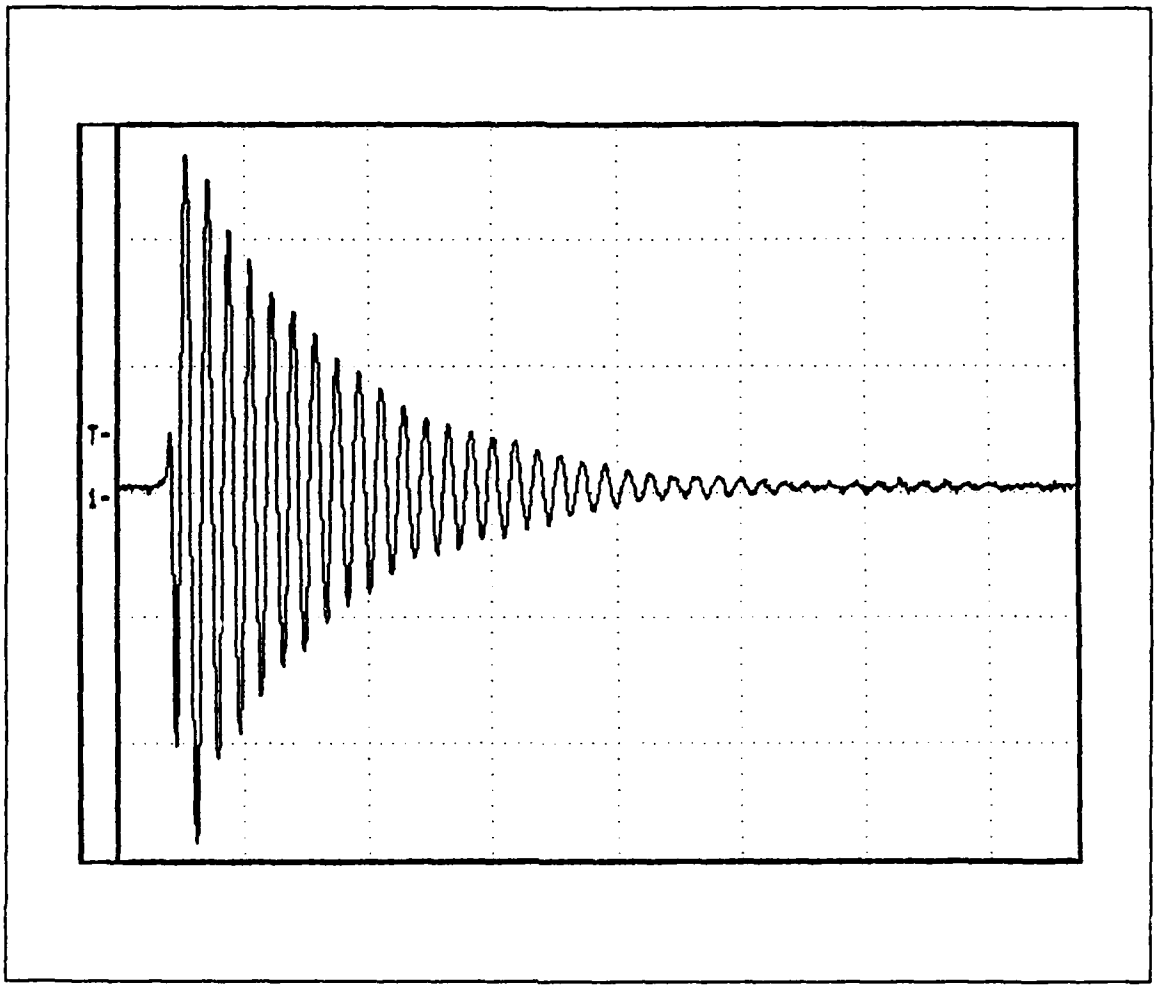

**Figure 7. Acoustic pressure caused by bubble:** The same bubble of Figure 5, with 200 microseconds between vertical grid members and the amplitude decreased by a factor of 2 to see the details.

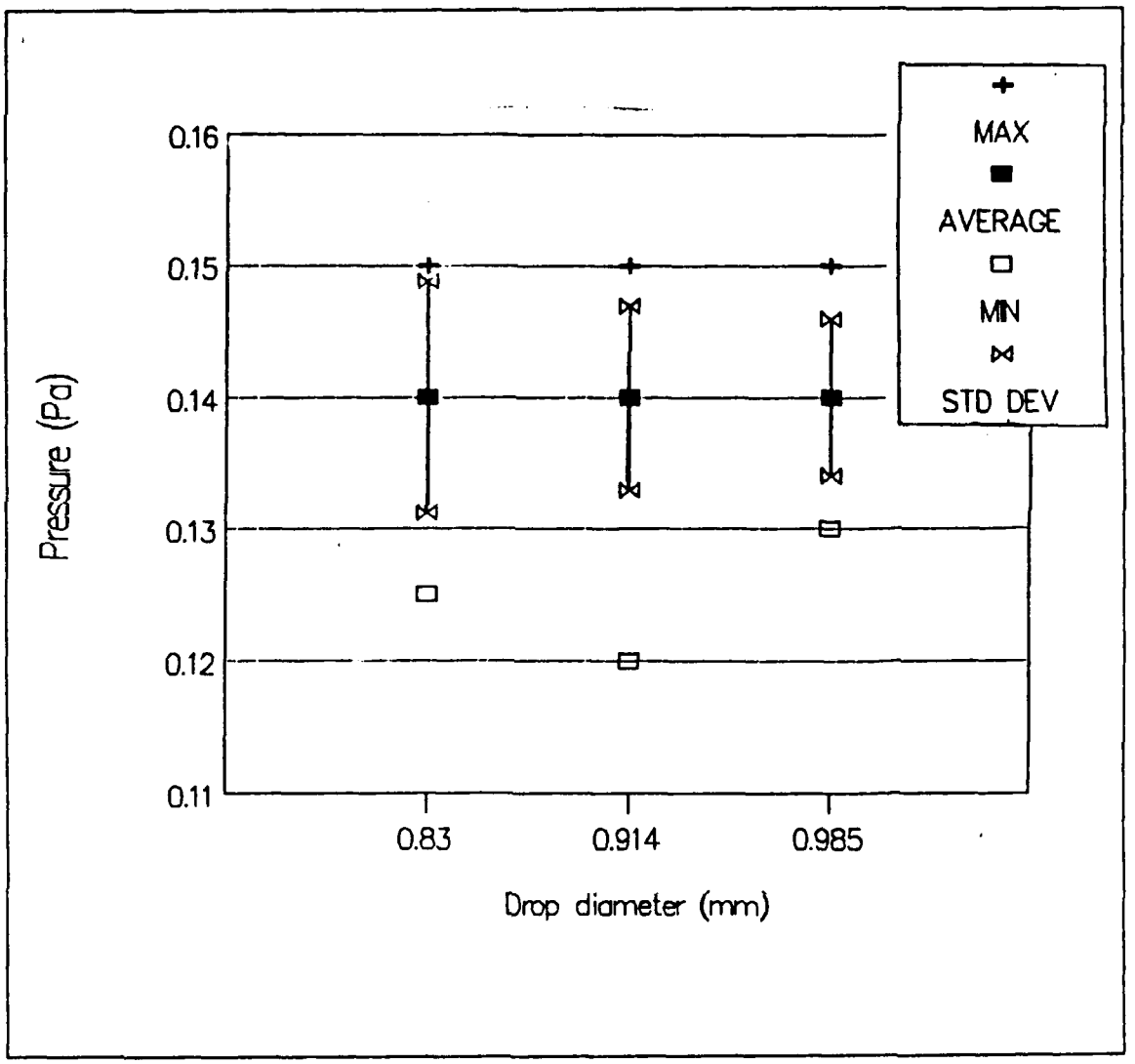


**Figure 8. Average peak axial pressures for impacts:** Maximum, minimum, average peak axial pressures and standard deviations of impacts for different drop sizes falling at normal incidence.

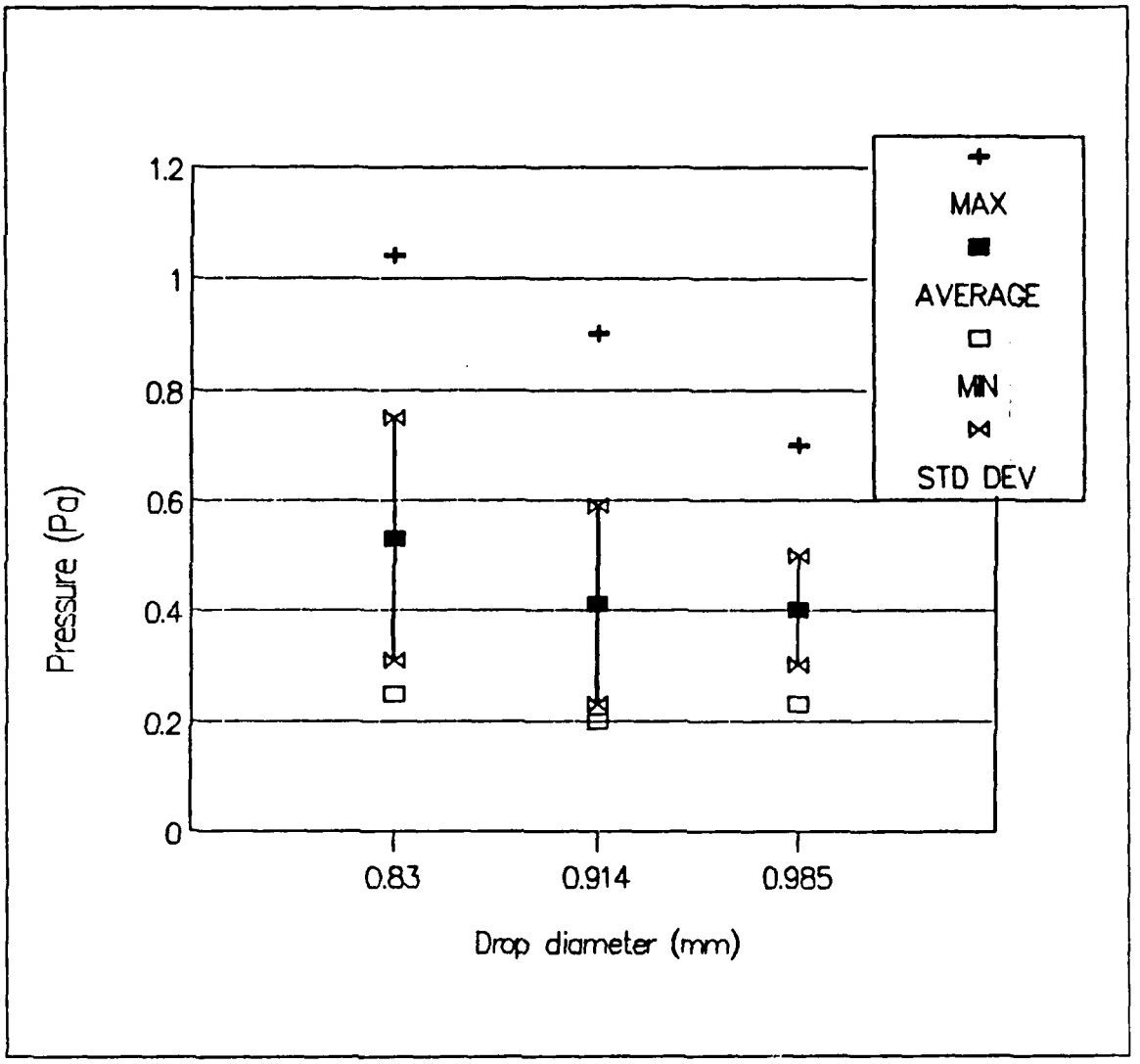


**Figure 9. Average peak axial pressures for bubbles:** Maximum, minimum, average peak axial pressures and standard deviations of bubbles for different drop sizes falling at normal incidence.

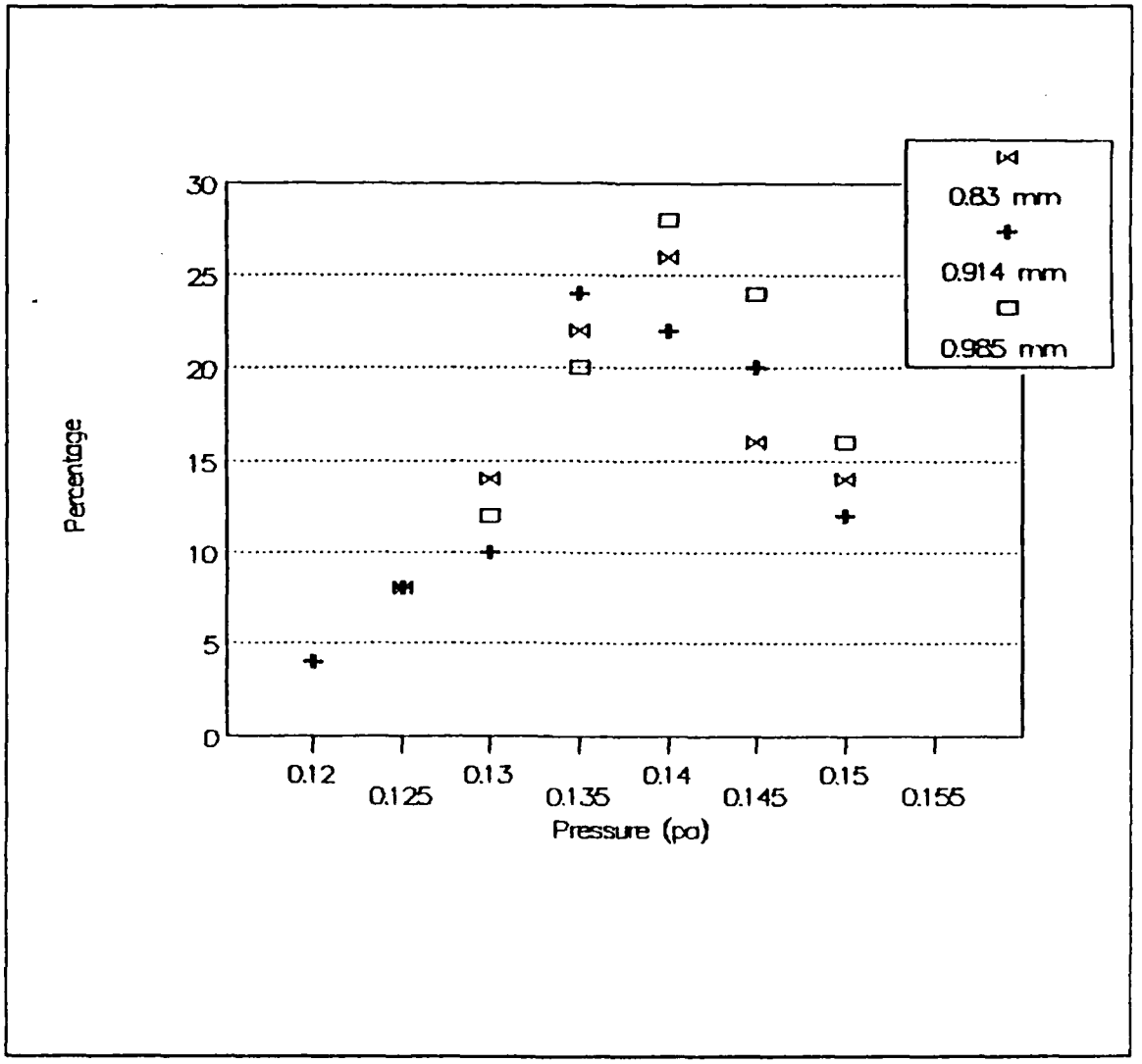


**Figure 10. Peak axial pressure histograms of impacts:** For 300 normal incidence drops. Since there were 100 of each size the vertical axis is both the percentage and the total numbers of peak impact pressures observed.

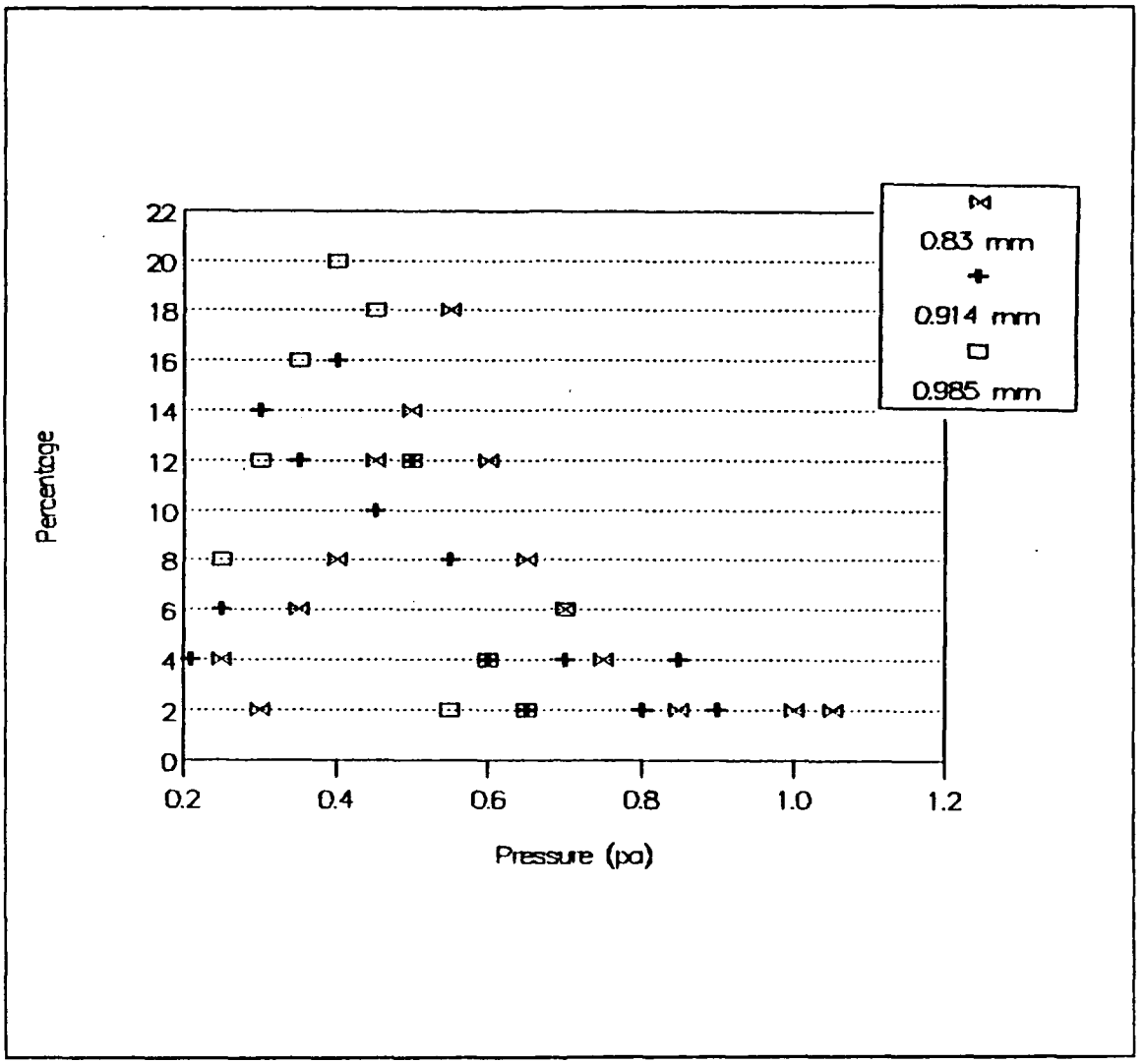


**Figure 11. Peak axial pressure histograms of bubbles:** For 300 normal incidence drops. Since there were 100 of each size the vertical axis is both the percentage and the total numbers of peak bubble pressures observed.

## 2. Total Acoustic Energy

Total acoustic energy radiated both by the bubble and the impact were calculated by using the formulas described in the previous chapter. The calculation of the radiated acoustic energies is as follows: for the impact we measured the output voltage at every 2 $\mu$ sec and converted this value to pressure using the formulation described in the previous section of this chapter. Then by using the energy formula given in Chapter 2 (Theory of the experiment), we found the acoustic energy radiated by the impact. We calculated the acoustic energy radiated by the bubbles first again using the output voltages every 2 $\mu$ second. Then for a simplified calculation we assumed a constant pressure equal to the each peak pressure for each half period cycle and calculated the energy for such an alternating square wave signal. This was compared with the energy calculated accurately for the 2 $\mu$ second recording using 20 bubbles as a test population, we found that the accurate calculation gave 67 % of the energy of the approximate square wave calculation. This value is very close the rms amplitude of each half cycle, which is 71 % of the peak amplitude. Based on this calculation we calculated the acoustic energies radiated by the bubbles by using only the peak pressures of the half cycles and taking the 67 % of the result obtained. For example, for one of the bubbles we studied, $p_{1ax}$ , the consecutive half cycle peak pressures, were 0.38, -0.5, 0.23, -0.19, 0.14, -0.15 etc. pascal with an oscillation period of 72 $\mu$ sec. Using the formula :

$$Energy = (2\pi \frac{R^2}{3\rho c}) \sum p_{1ax}^2 \Delta t$$

where the squared pressures are 0.14, 0.258, 0.055, 0.04, 0.02 etc. $Pa^2$ , $\Delta$ t = 36 $\mu$ second, R = 20 cm, and $2\pi \frac{R^2}{3\rho c} = 5.66 \times 10^{-8}$ The sum of squared pressures is 0.6 $Pa^2$ and therefore the energy is $1.06 \times 10^{-12}$ joule.

The average values for the impact and bubble acoustic noise are shown in Figures 12 and 13, with standard deviations and with maximium and minimum energies obtained for three different drop sizes. The energy histograms for impacts and bubbles obtained during the normal incidence experiment are also shown in Figures 14 and 15. The ratio of the total average acoustic energy (impact and the bubble) to the calculated

kinetic energy of the drops just before the impact is $1.43 \times 10^{-6}$ for 0.83 mm diameter drops, $6.6 \times 10^{-7}$ for 0.914 mm and $4.51 \times 10^{-7}$ for 0.985 mm diameter drops. Where the Kinetic energies are $1.58 \times 10^{-6}$ Joule for 0.83 mm, $2.74 \times 10^{-6}$ Joule for 0.914 mm and $3.61 \times 10^{-6}$ Joule for 0.985 mm diameter drops.

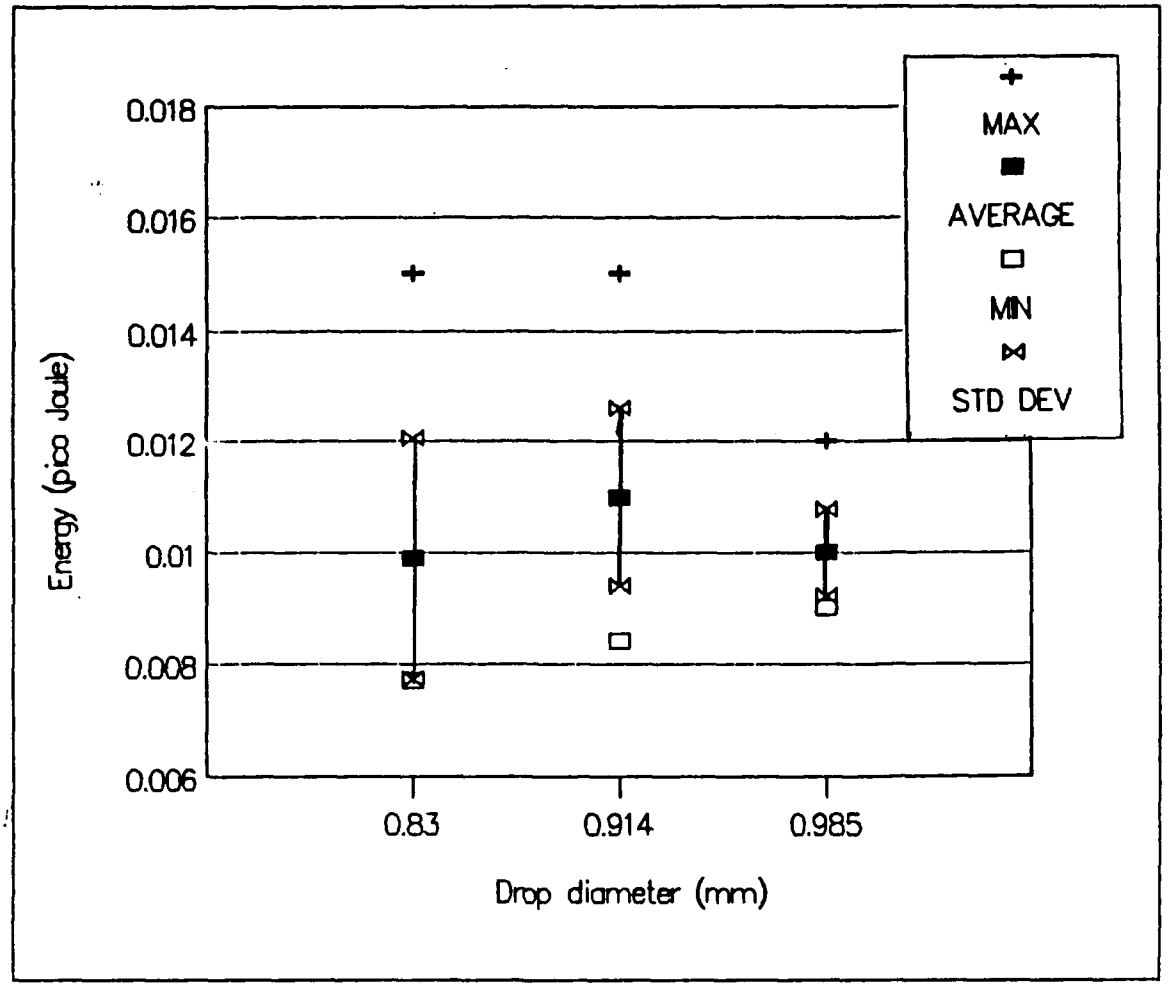


**Figure 12. Average acoustic energies radiated by the impacts:** Average, maximum and minimum energies with standard deviation for normal incidence drops

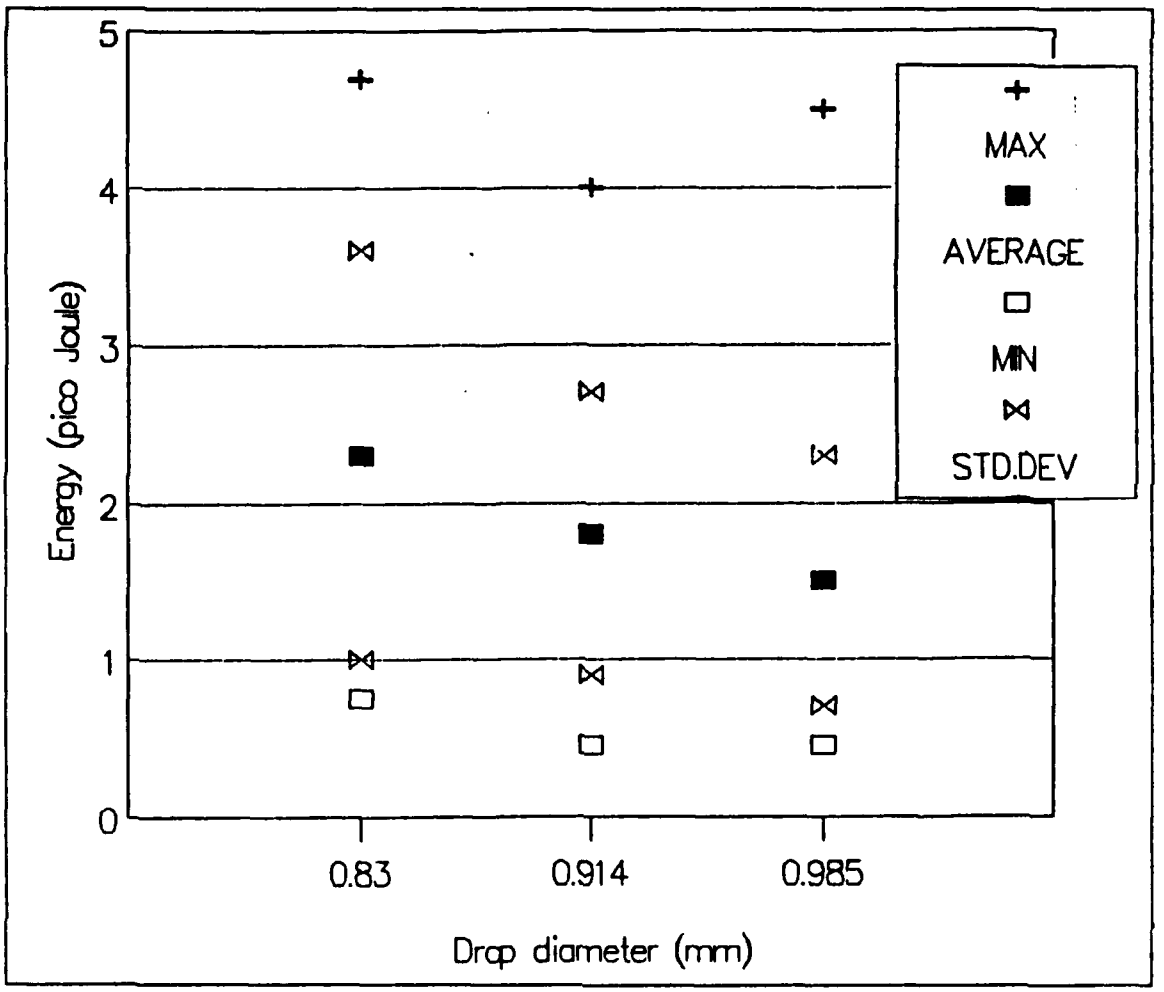


**Figure 13. Average acoustic energies radiated by the bubbles:** Average, maximum and minimum energies with standard deviations for normal incidence drops

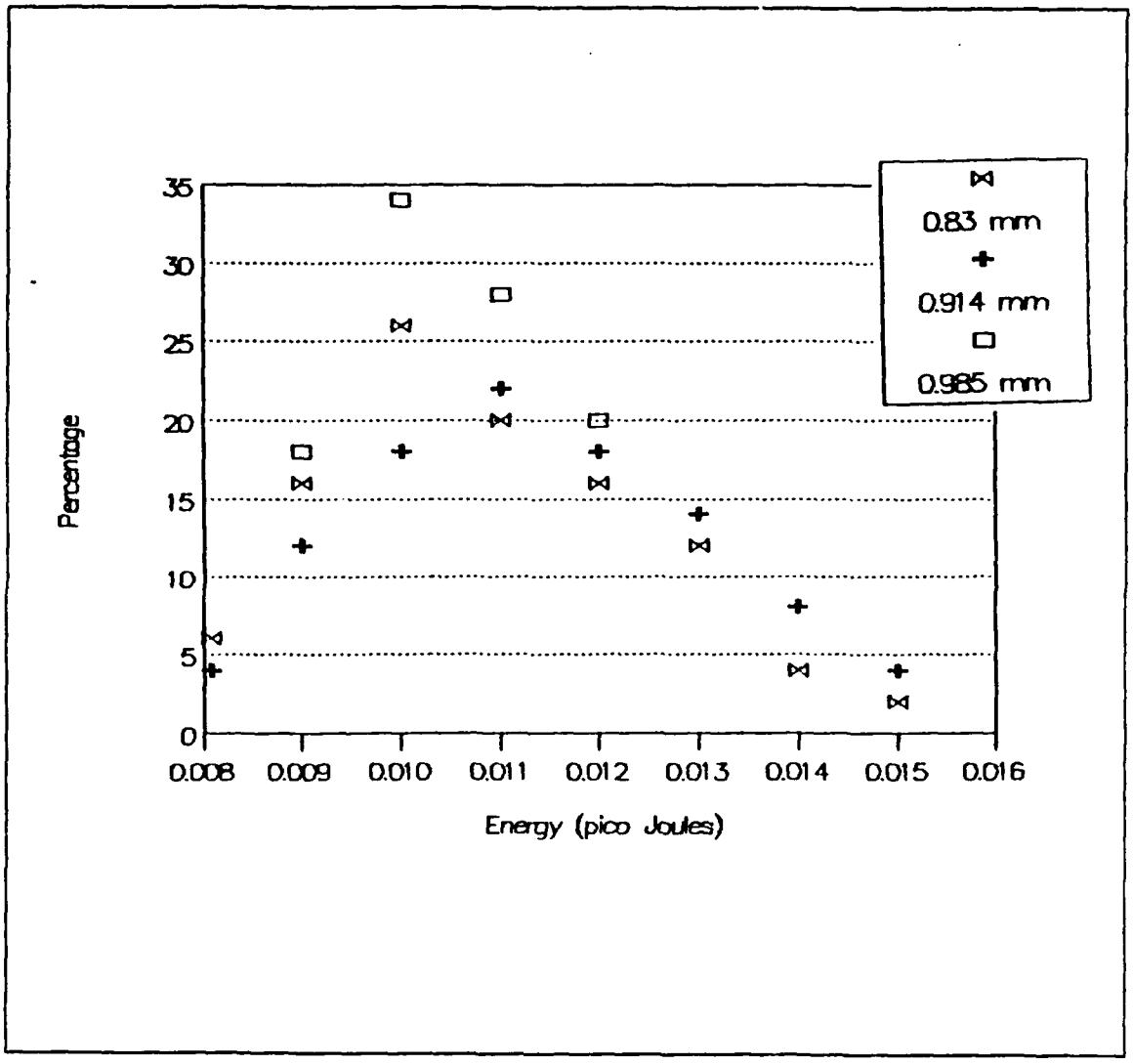


**Figure 14. Acoustic energy histograms of the impacts:** Acoustic energies for 300 drops (100 of each size) at normal incidence and terminal velocities.

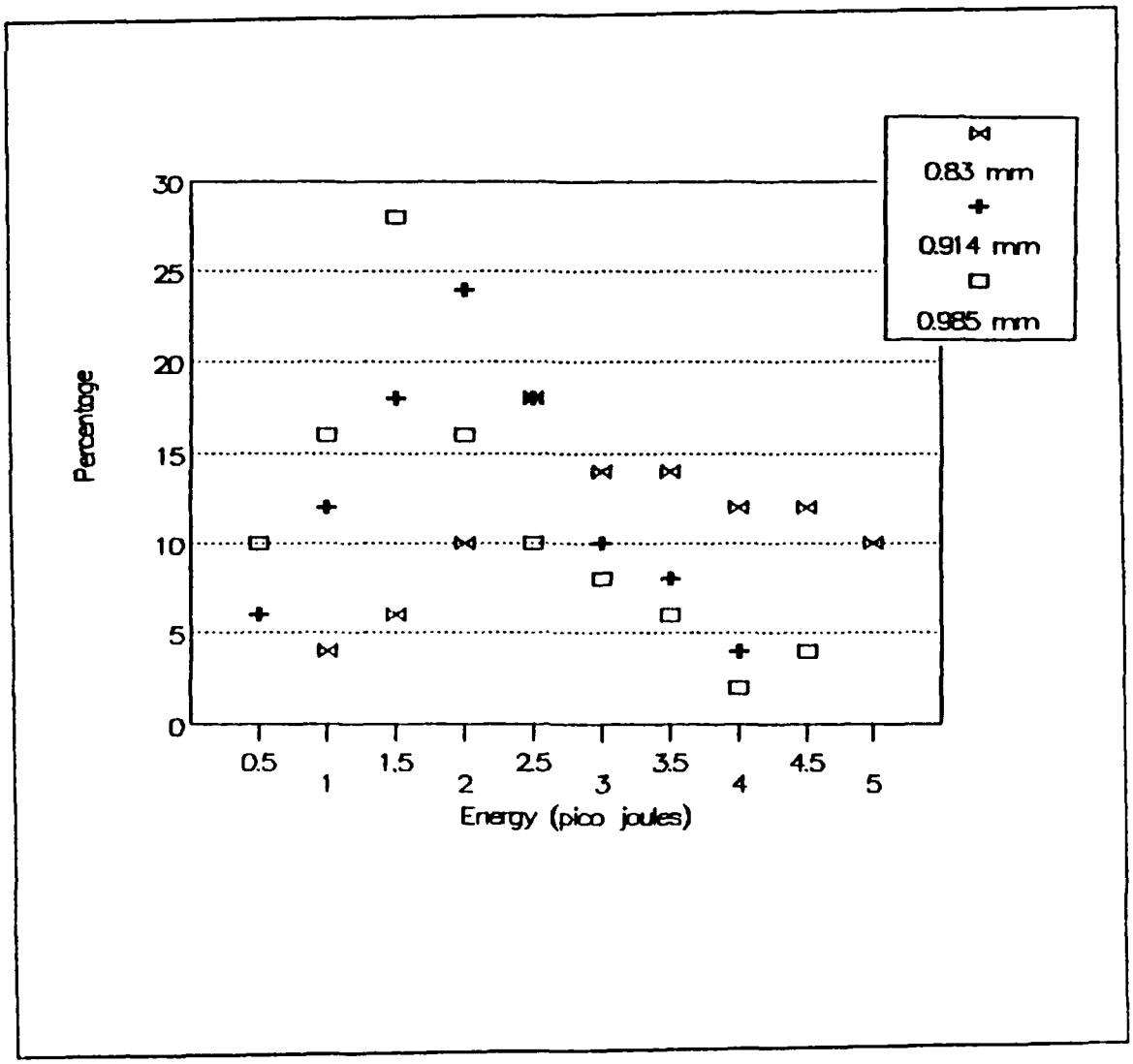


**Figure 15. Acoustic energy histograms of the bubbles:** Acoustic energies for 300 drops (100 of each size) at normal incidence and terminal velocities.

### 3. Frequency Specta

The central frequency for the impact was found by taking its Fourier Transform. A frequency spectrum of impact noise for a normally incidenting 0.83 mm diameter drop is shown in Figure 16. Histograms of the impact peak frequency for 0.83 to 0.985 mm diameter, normal incidence drops, falling with their terminal velocities are shown in Figure 17. Because the impact signal approximates a doublet (two opposed delta functions), its spectrum is very broad. Its peak at about 15 kHz agrees with the prediction by Nystuen (1986).

The bubbles are similar to Type A1 bubbles in breaking waves (Medwin and Beaky, 1989), which were described as simply damped spherical bubbles. The period is easily found by measuring the duration between two consecutive peaks. The frequency is found simply by taking the reciprocal of the period. The resonance frequencies of the bubble radiation for different sizes of drops are shown in Figure 18.

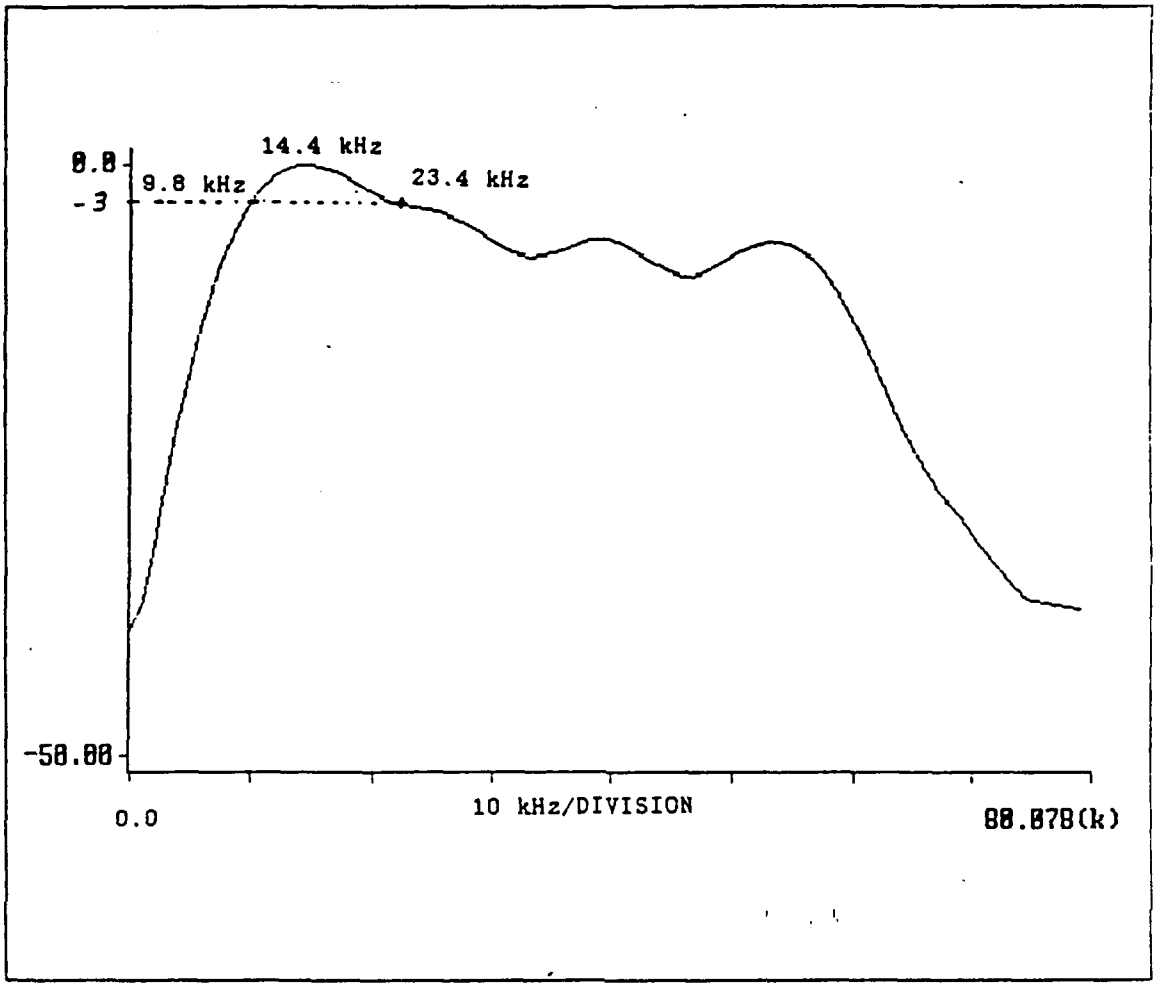


**Figure 16. Frequency spectrum of the impact sound.:** For a 0.83 mm (diameter) drop normally incidenting with its terminal velocity.

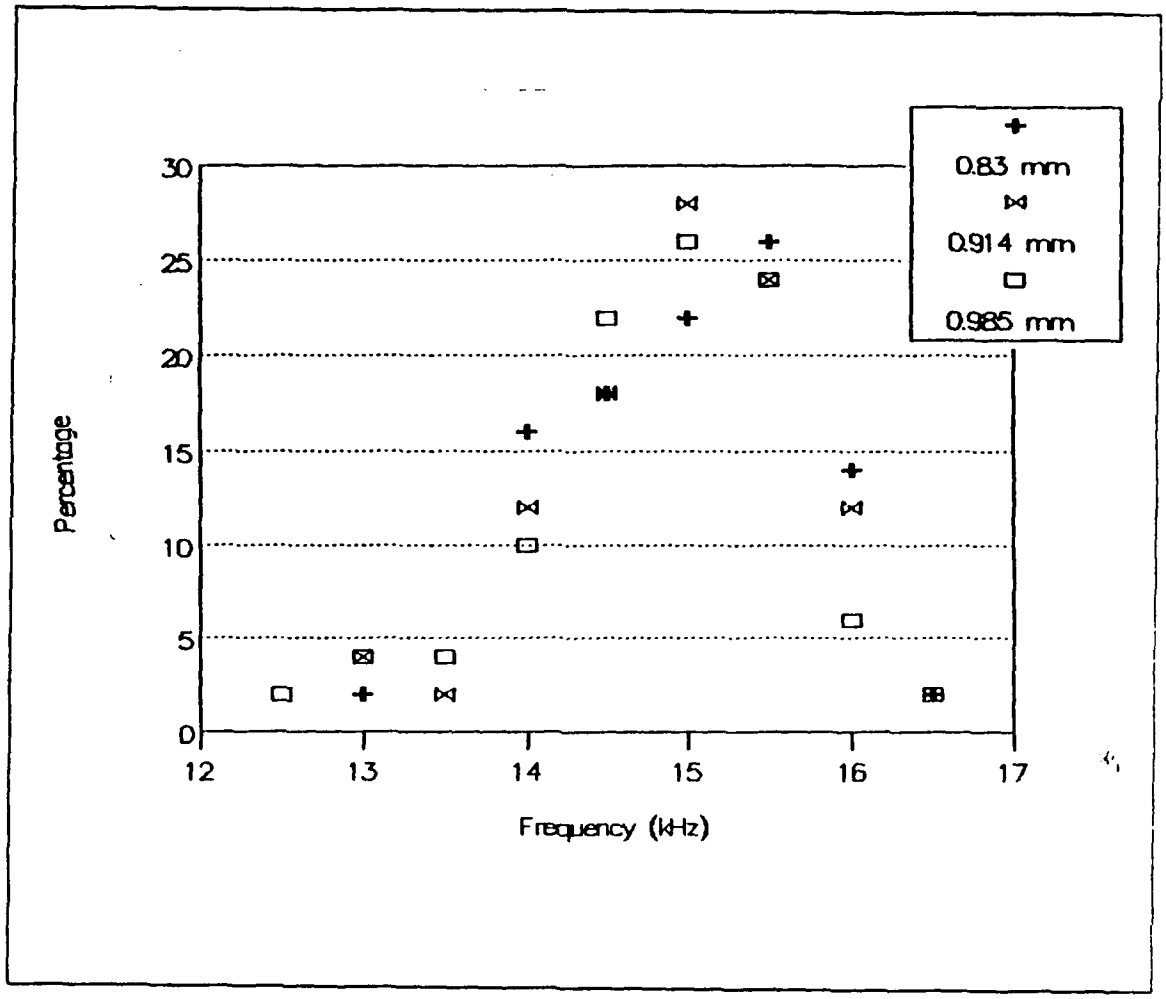


**Figure 17. Peak frequencies of impacts:** For 150 normal incidence drops (50 of each size).

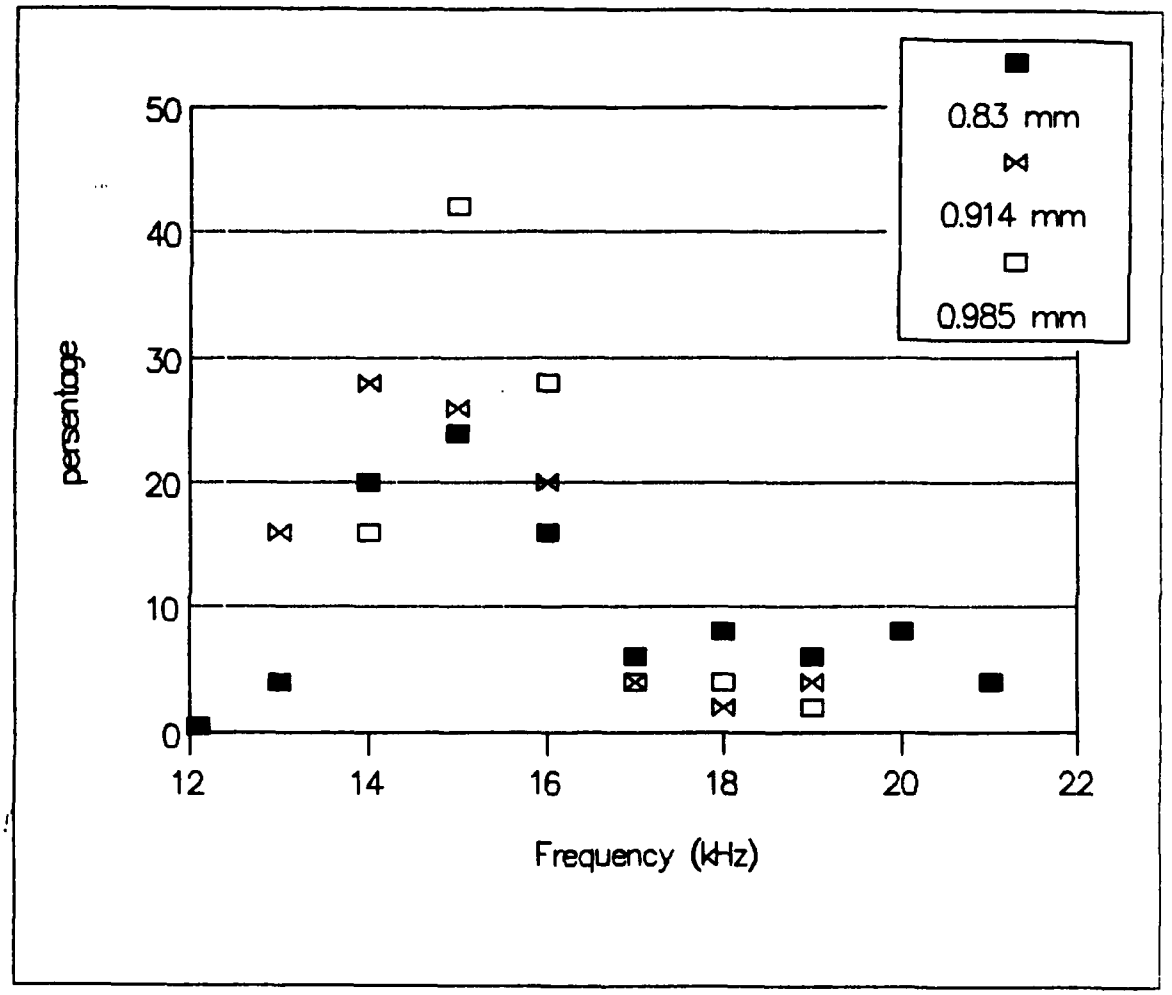


**Figure 18. Resonance frequencies of bubbles:** For 150 normal incidence drops (50 of each size).

## 4. Radiation Pattern

To find out the radiation pattern of the impact and the bubble noises we first used the 8 hydrophone array shown in Figure 19, with the hydrophones placed every 20 degrees on each side of the vertical axis with a highly sensitive hydrophone on the center for triggering. First it was verified that the polar radiation pattern is nearly same as the theoretical dipole radiation pattern, which is the $p_{ox}\cos\theta$ as described in the previous chapter. Since the pressure on both sides of the axis was verified to be symmetric, the array was changed as shown in Figure 20, with hydrophones placed only on one side of the axis with 10 degrees between them to provide a more accurate beam pattern.

The polar radiation patterns for normal incidence drops of different sizes are as shown in Figure 21 including their theoretical radiation patterns. As we can see from Figure 21, the radiation pattern is not an exact dipole but is very close to a dipole.

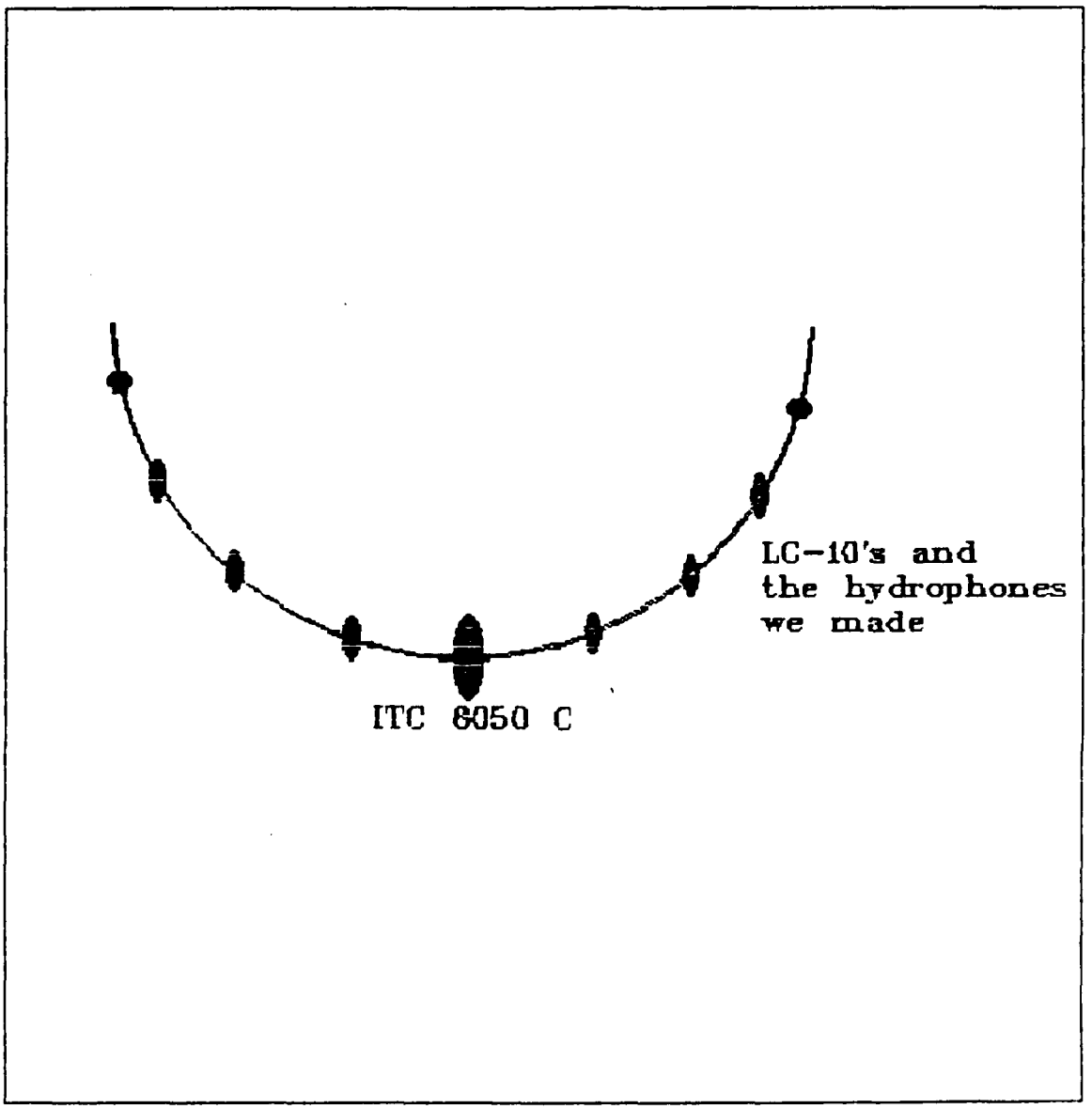


Figure 19. Eight hydrophone array with 20 degere separations

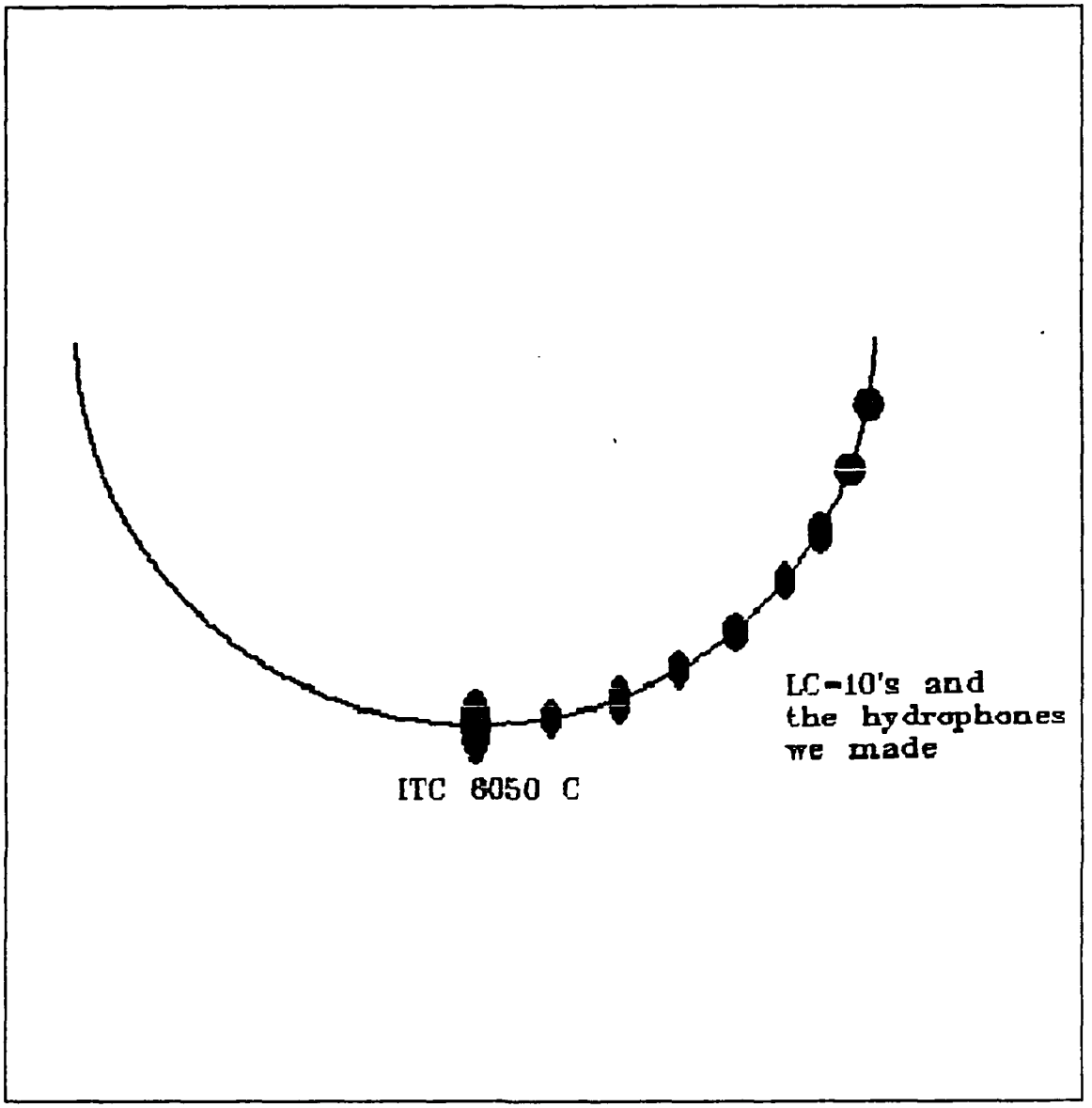


Figure 20. Eight hydrophone array with 10 degree separations

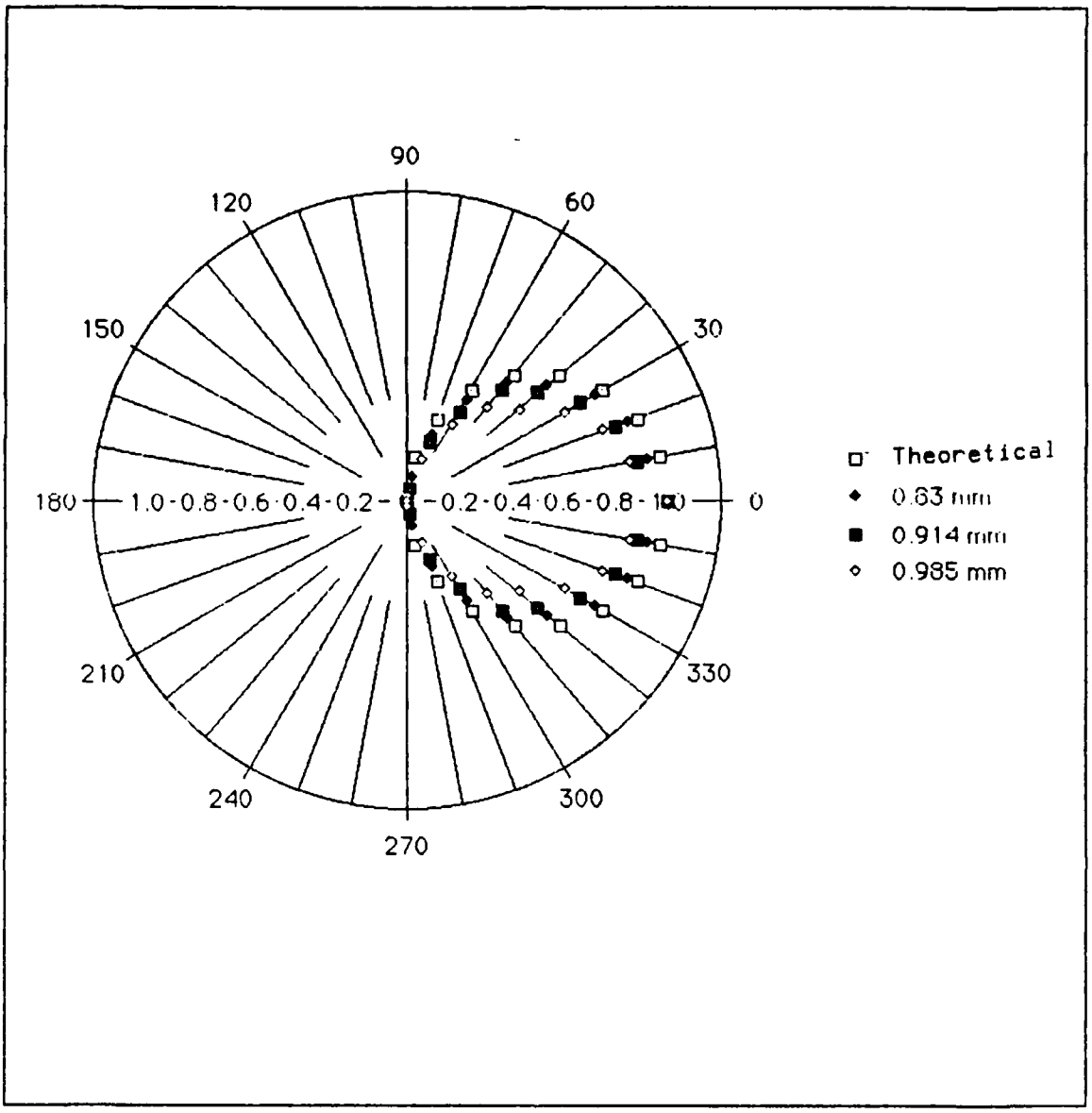


**Figure 21. Polar radiation pattern of normal incidence drops:** Polar radiation pattern for 0.3 $\mu$ l (0.83 mm diameter), 0.4 $\mu$ l (0.914 mm) and 0.5 $\mu$ l (0.985 mm) drops at normal incidence and terminal velocity compared with theory.

## C. OBLIQUE INCIDENCE

The same experimental procedure used for normal incidence drops was followed to record and observe the acoustical properties of impacts and entrained bubbles for oblique incidence drops. A fan was used to impart a horizontal velocity. To obtain the angle of incidence and the impact velocity two different methods were used. The first technique was to take still photographs of drops in their path by using a stroboscope calibrated to a certain frequency and measuring the distance the drop travelled between two consecutive flashes of the stroboscope. This value was divided by the time between two consecutive flashes to find the velocity of the drops. A 5 cm x 5 cm string grid was used behind the path of the drops to obtain maximum accuracy. The angle of incidence was measured by using the same grid. The second technique was to take a motion picture of the drops using a video camera. Drop angles and velocities were then obtained by using a video recorder that has the capability of slow motion (frame by frame) with adjustable speed. We mostly used the second technique which made the observation of the angle and the impact velocity much easier. To measure the distances for the second technique again the string grid was used.

### 1. Peak Axial Pressure

The peak axial pressure for the bubbles and the impacts of different sizes of drops were measured for different incidence angles. The axis is again defined as being perpendicular to the water surface. The average pressures are shown in Figures 22 and 23, for different drop sizes and different angles of incidence.

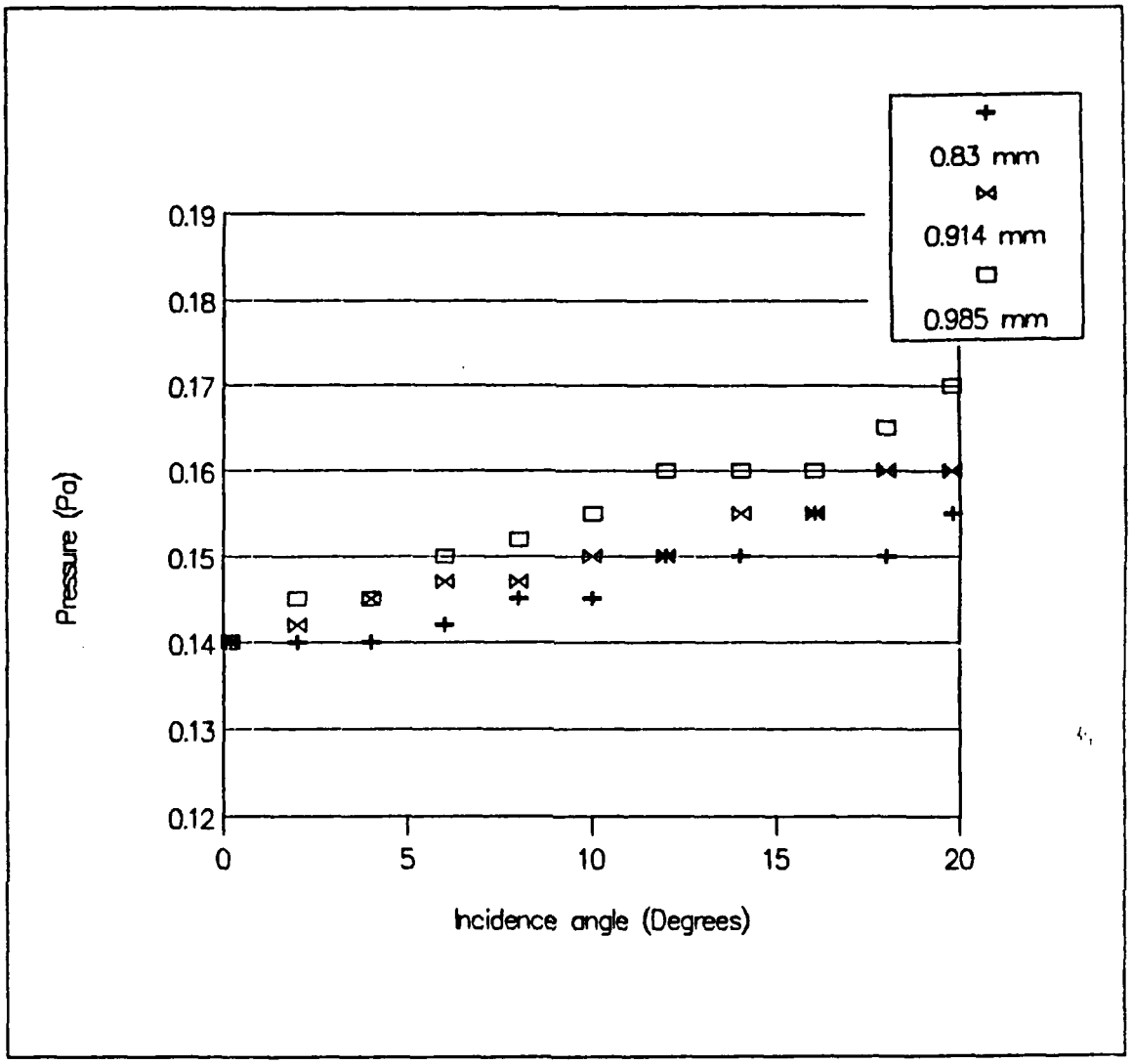


**Figure 22. Average peak axial pressures for impacts:** For different drop sizes as a function of incidence angle.

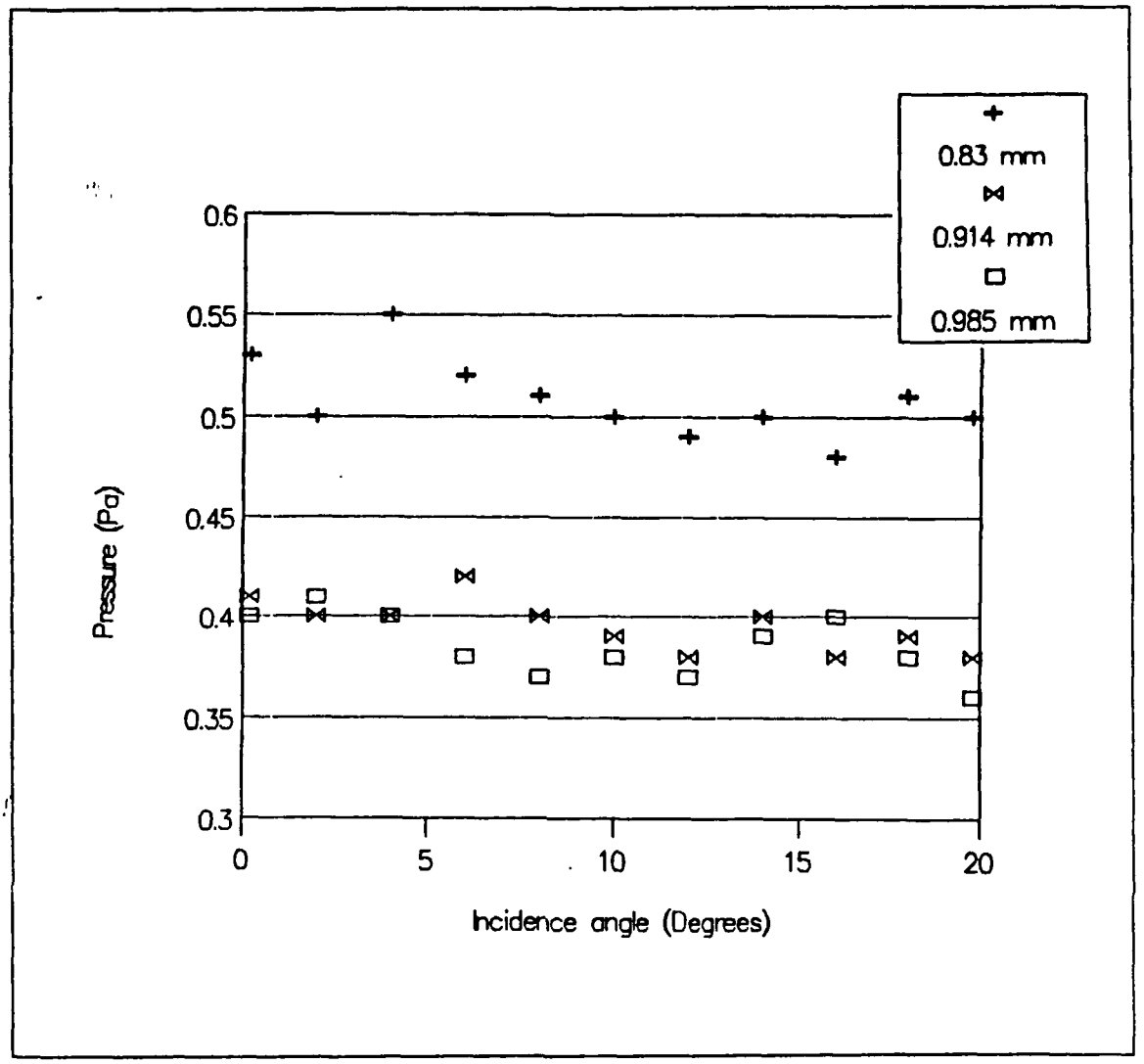


**Figure 23. Average peak axial pressures for bubbles:** For different drop sizes as a function of incidence angle.

## 2. Total Acoustic Energy

Total acoustic energy radiated both by the bubble and the impact were calculated by using the formulas described in the previous chapter for a dipole perpendicular to the surface. The maximum, minimum and average acoustic energies are shown in Figures 24 to 26. The average acoustic energies radiated by the oblique impacts of different drop sizes are shown in Figure 27. It was observed that at high incidence angles the energy radiated by the impact increases as can be seen from Figure 27.

Maximum, minimum and average energies radiated by oblique incidence bubbles for different drop sizes are shown in Figures 28 to 30. Average energies radiated by bubbles of different drop sizes are as shown in Figure 31. As we can see from this figure average acoustic energies of bubbles do not change significantly with incidence angle. For all these figures, around 450 drops that created bubbles are used (around 150 for each size).

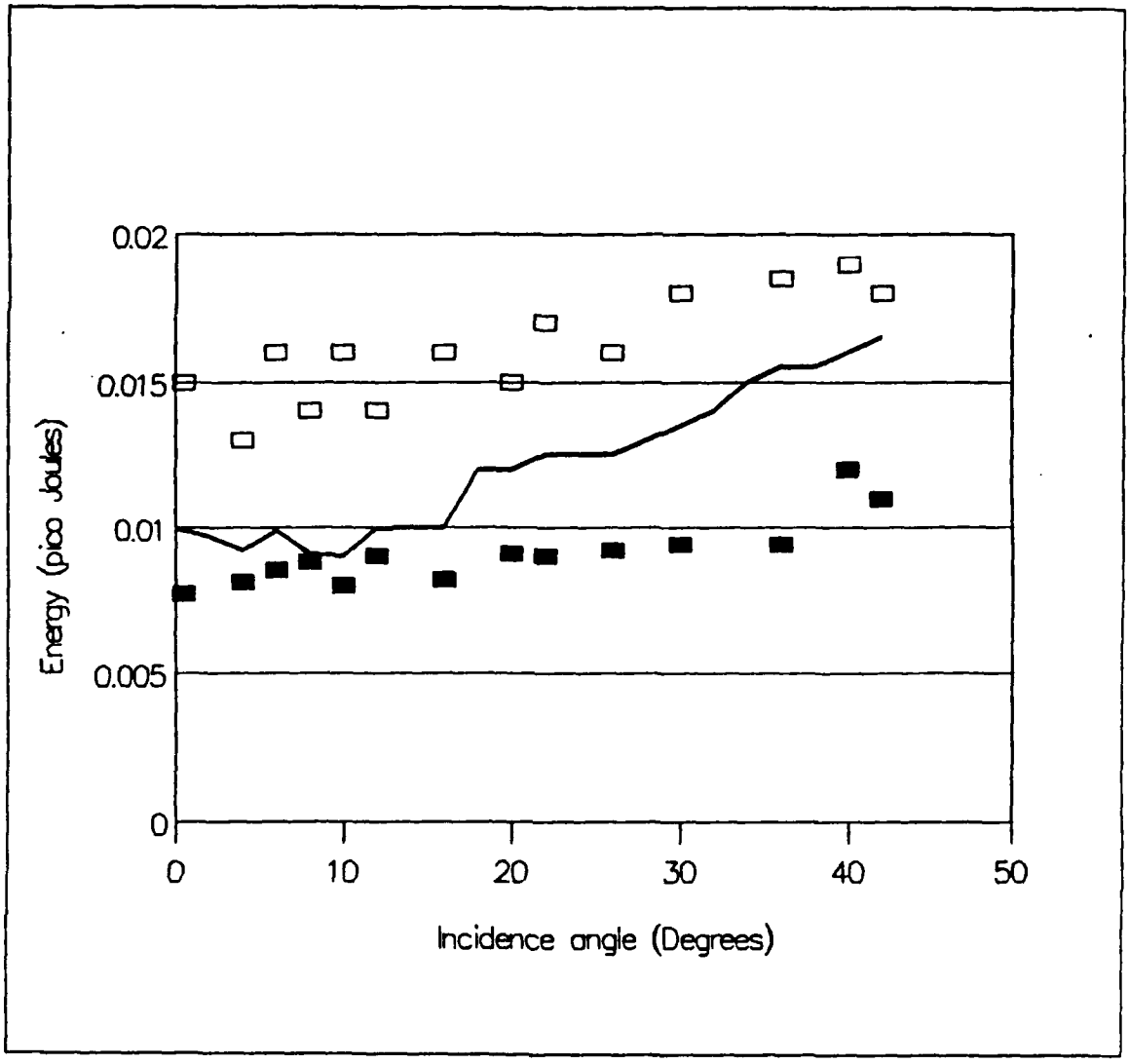


Figure 24. Max. min. and avg. impact acoustic energies for 0.83 mm drops

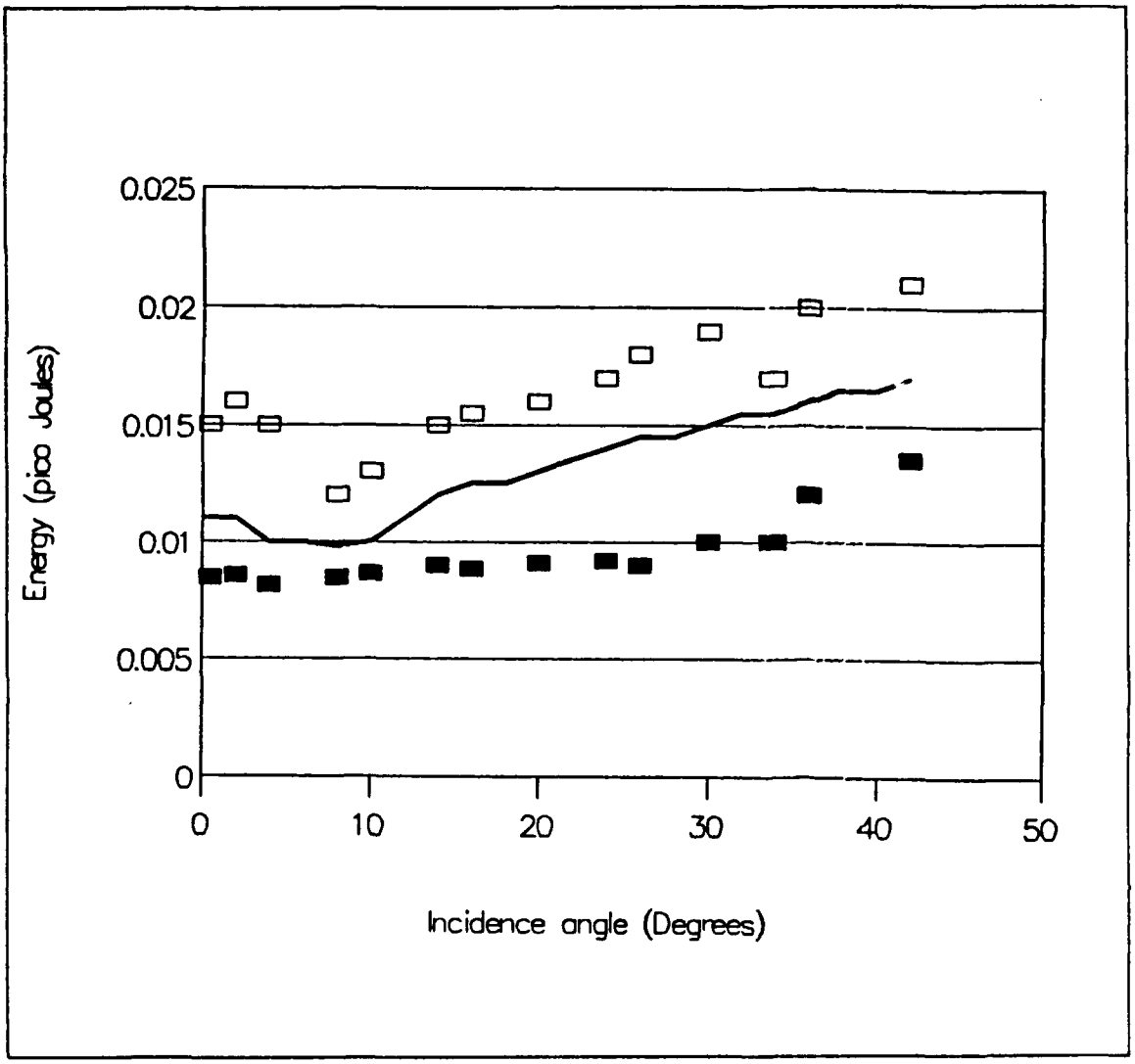


Figure 25. Max. min. and avg. impact acoustic energies for 0.914 mm drops

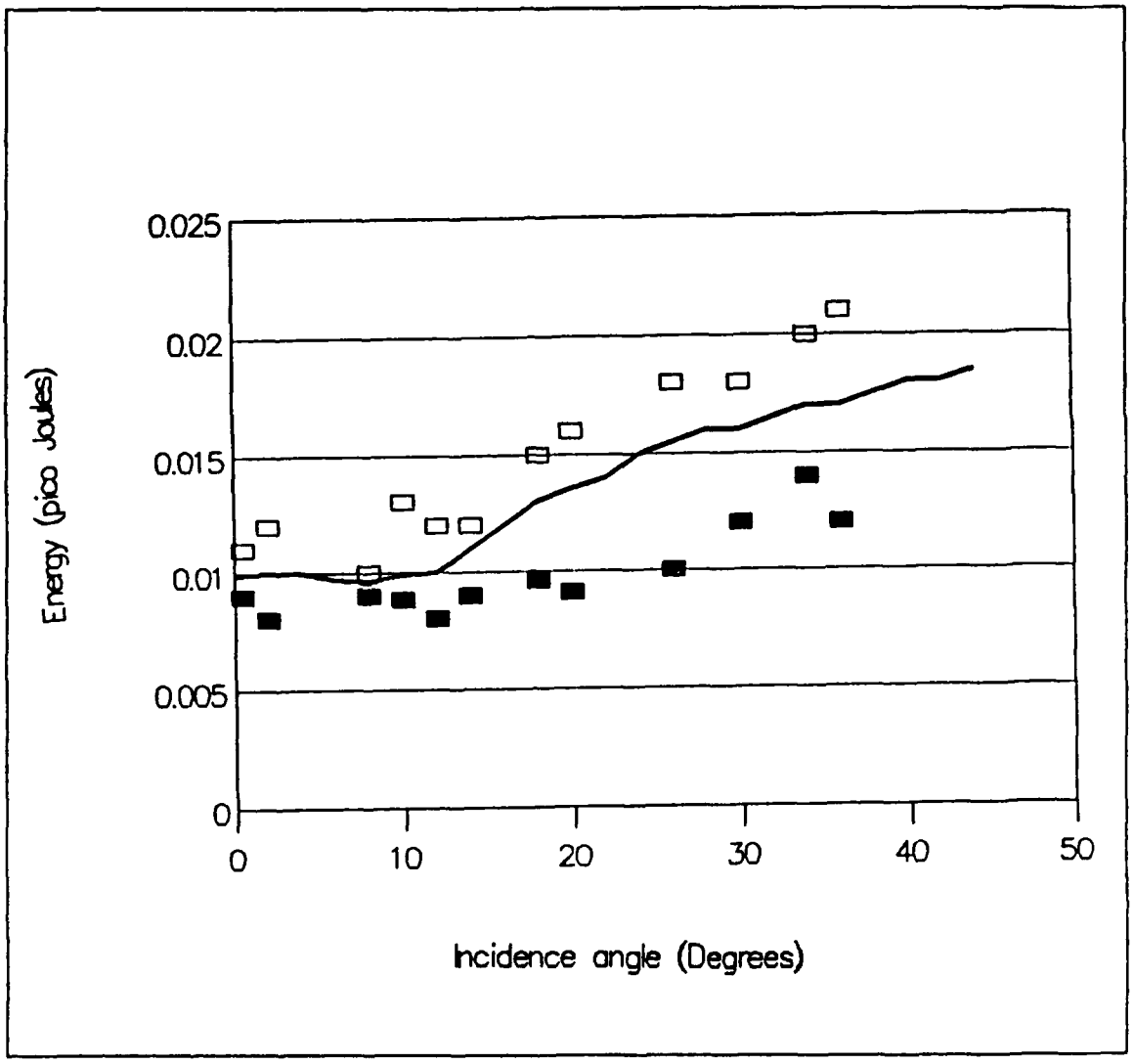


Figure 26. Max. min. and avg. impact acoustic energies for 0.985 mm drops

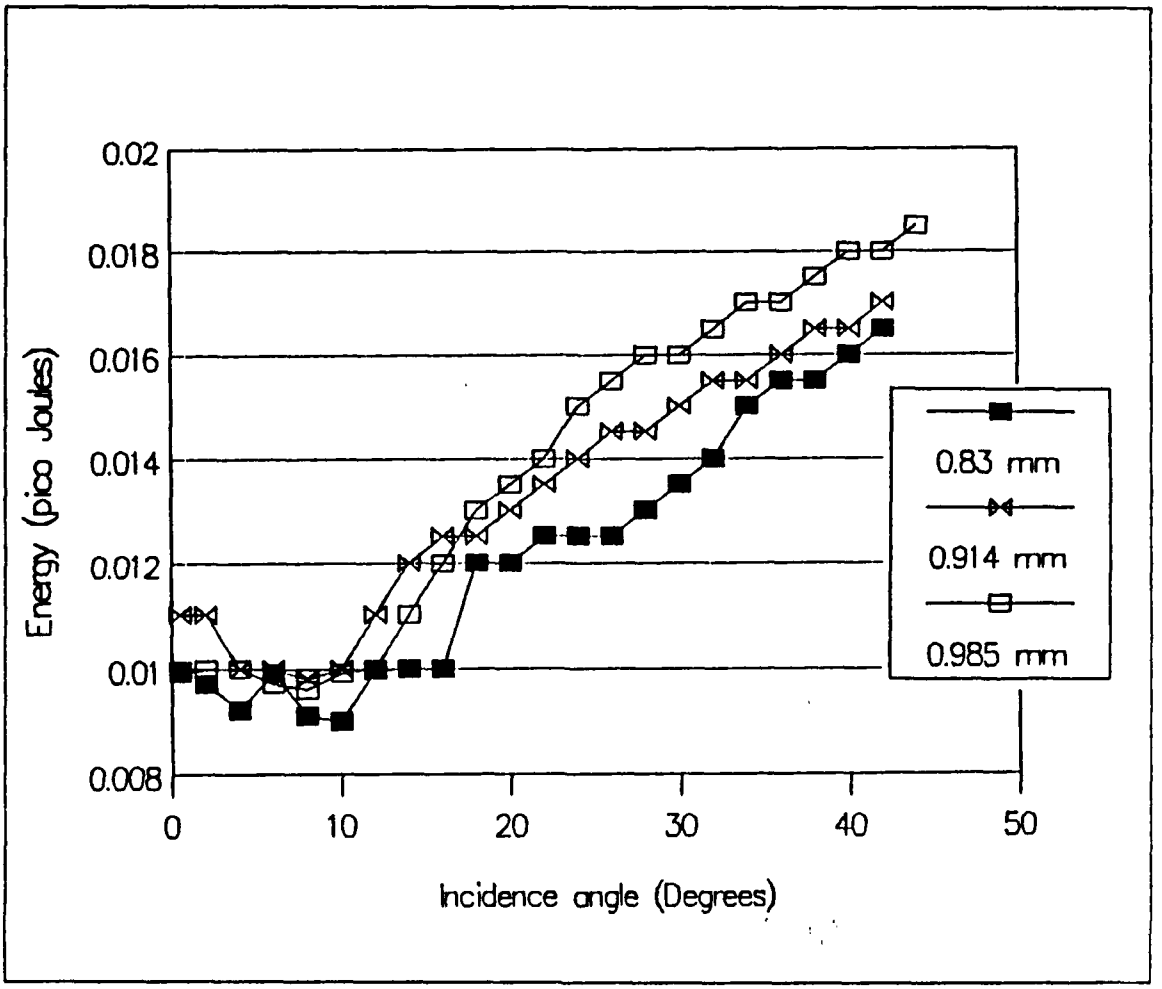


**Figure 27.** **Average impact acoustic energies of the drops** at oblique incidence

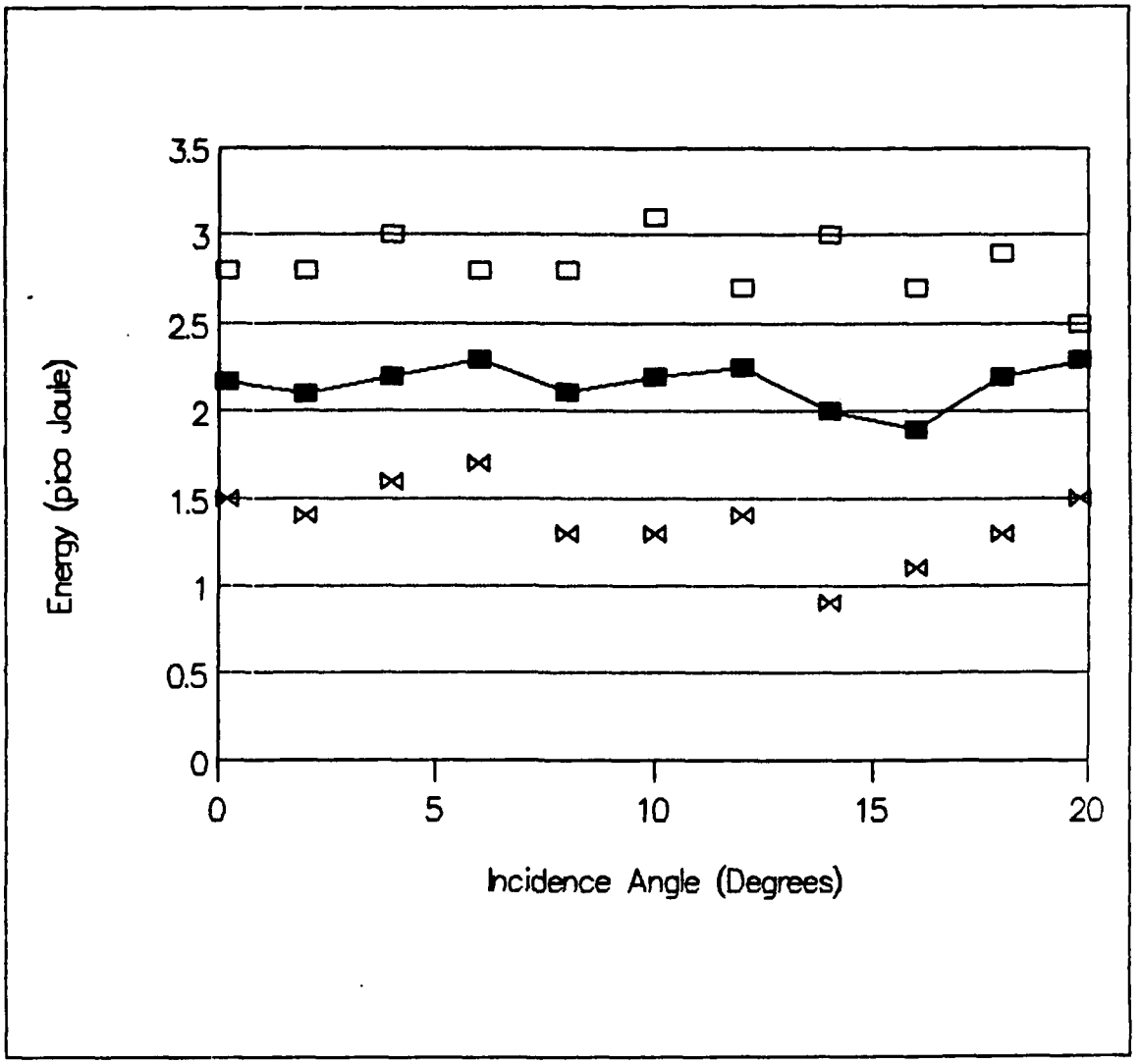


**Figure 28. Radiated bubble energy for 0.83 mm drops:** Maximum, minimum and average acoustic energy radiated by the bubbles of oblique incidence drops, observed for different incidence angles.

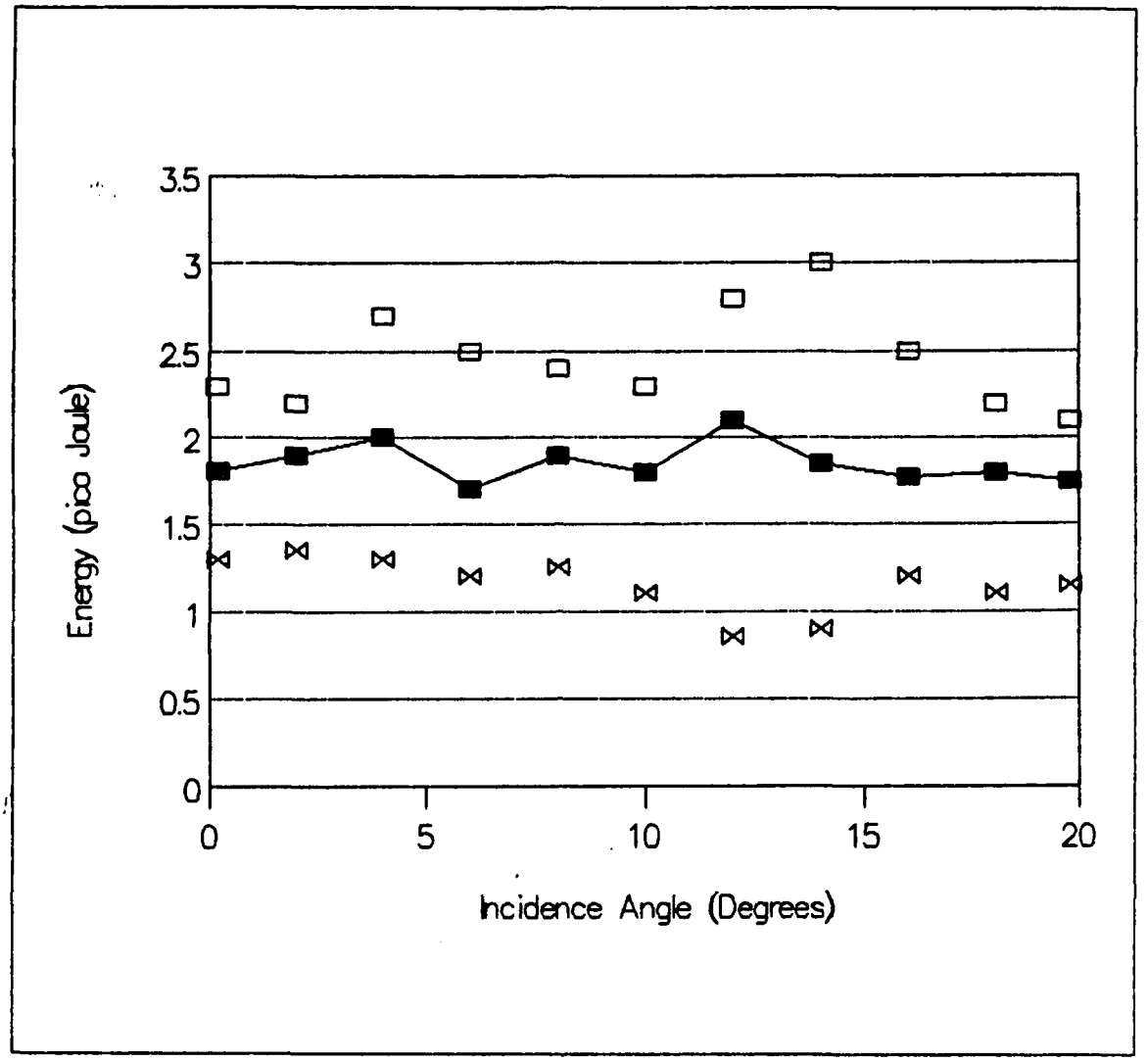


**Figure 29. Radiated bubble energy for 0.914 mm drops:** Maximum, minimum and average acoustic energy radiated by the bubbles of oblique incidence drops, observed for different incidence angles.

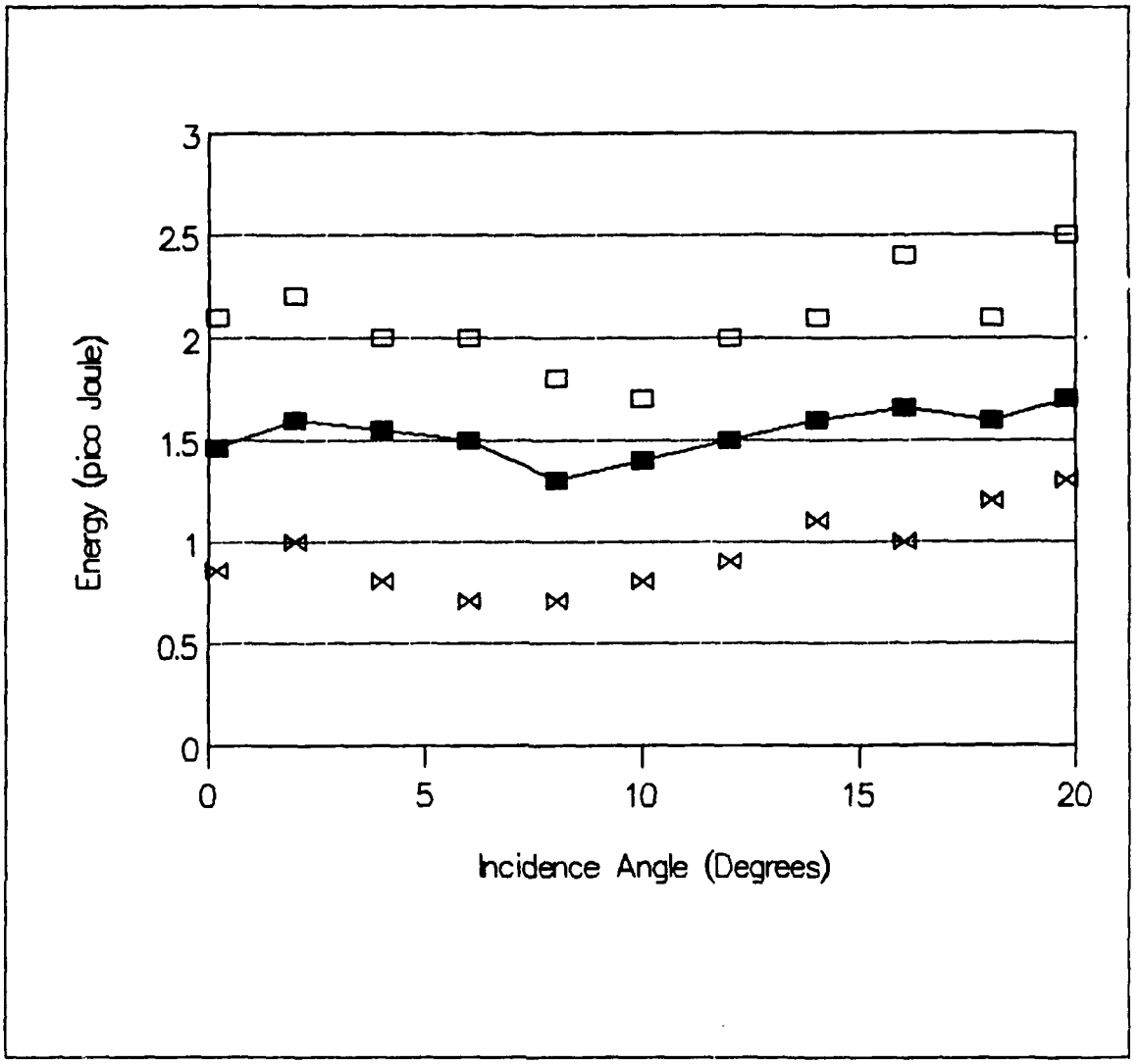


**Figure 30. Radiated bubble energy for 0.985 mm drops:** Maximum, minimum and average acoustic energy radiated by the bubbles of oblique incidence drops, observed for different incidence angles.

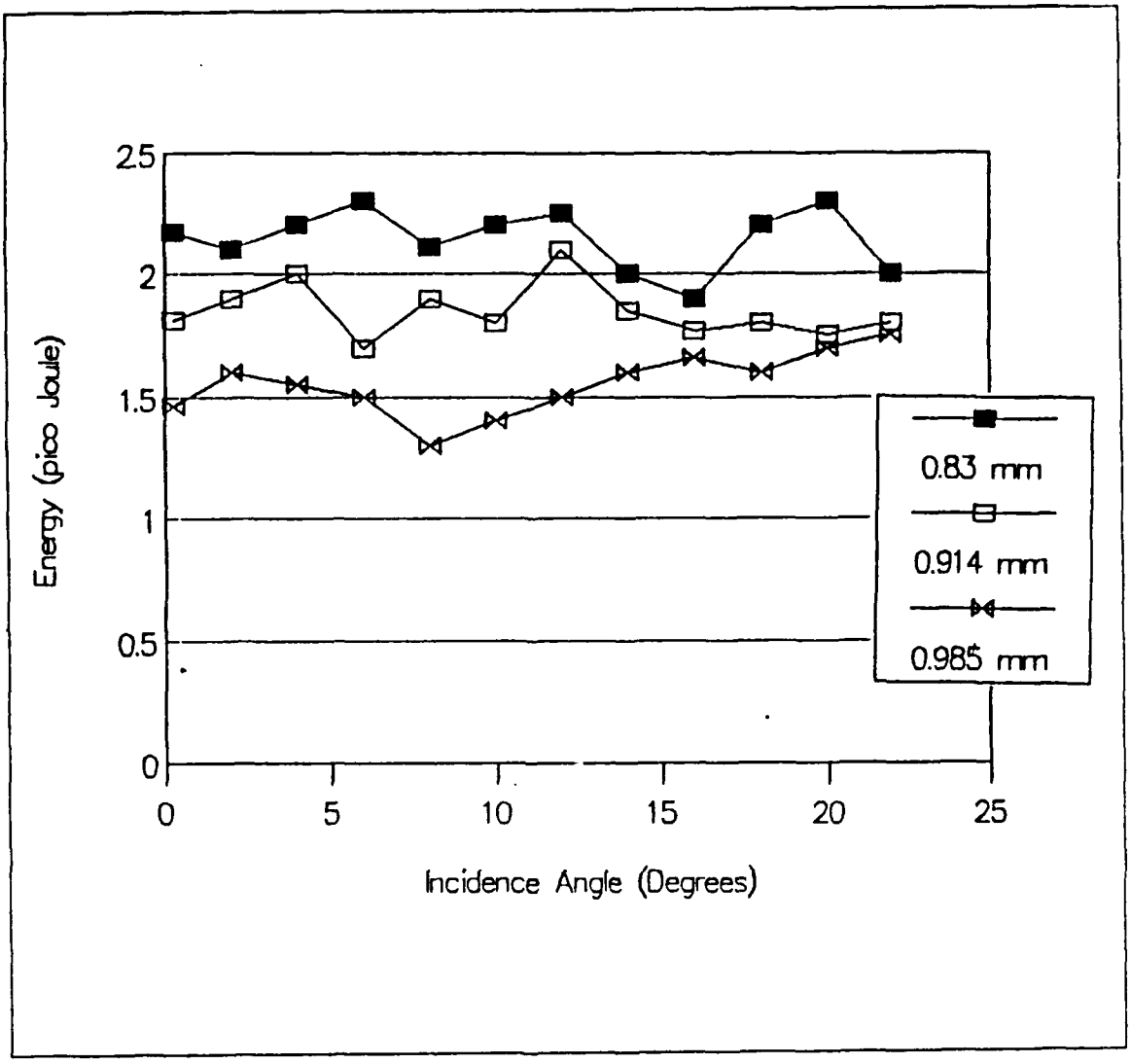


Figure 31. Average bubble acoustic energies for oblique incidence

### 3. Frequency Spectra

The spectrum for the impact was found by taking the FFT as in the normal incidence case. The frequency spectrum of a typical impact at oblique incidence is shown in Figure 32. Impacts of all drop sizes in our range (0.3 $\mu$ l to 0.5 $\mu$ l, or in other terms 0.83 mm to 0.985 mm diameter) had broad spectral peaks of nearly at the same frequencies for all different incidence angles. The peak frequency shifted slightly to lower frequencies for oblique incidence with respect to the normal incidence case. The average peak frequencies of the impacts is shown in Figure 33.

Frequencies of bubbles were found from the period of the bubbles, following the same method as used for normal incidence.

The range of resonance frequencies of bubbles for 0.83 to 0.985 mm drops for oblique incidence are as shown in Figures 34 to 36. The average frequencies of the bubble radiation for different sizes of drops and for different incidence angles are shown in Figure 37.

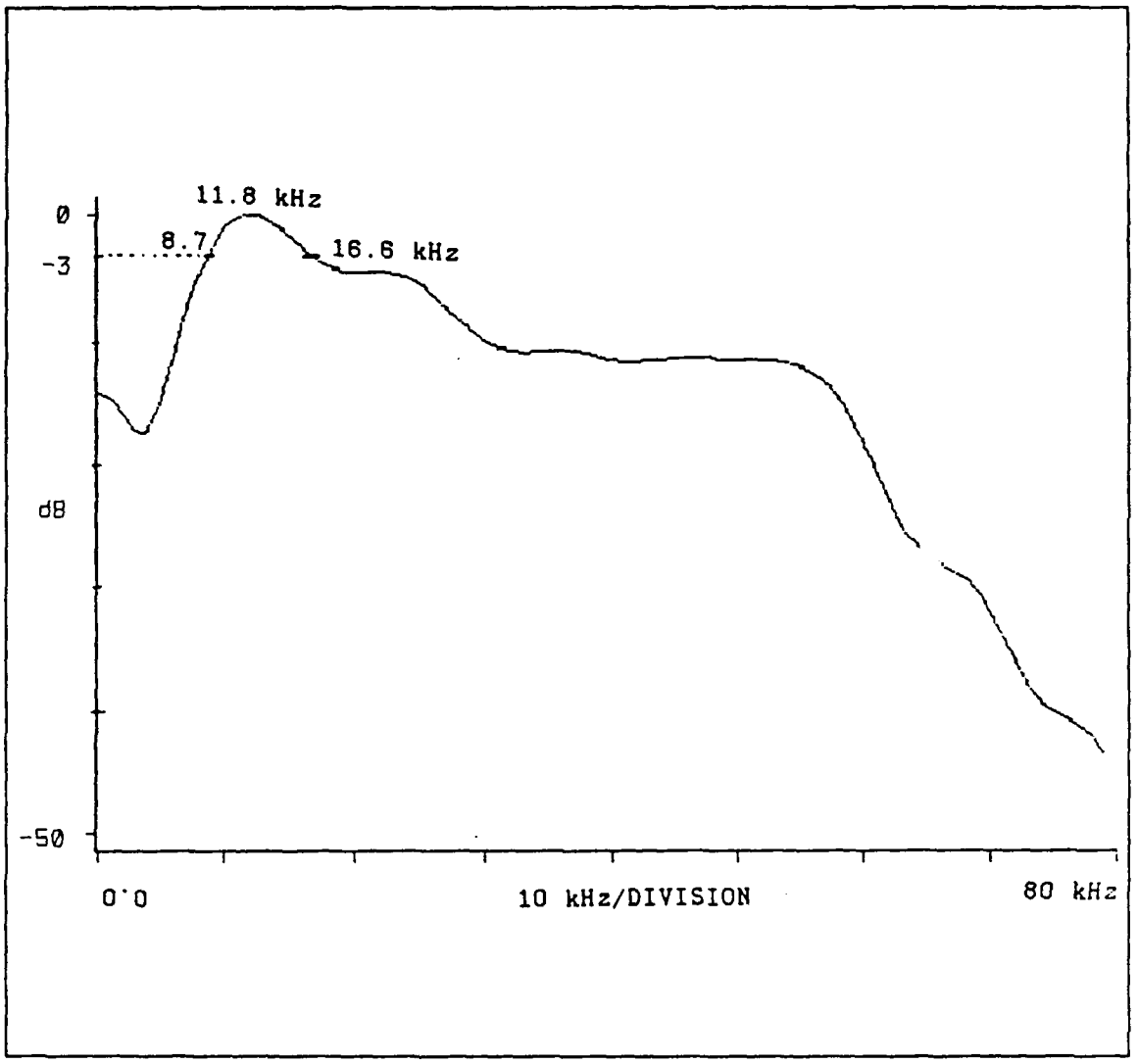


**Figure 32. Frequency spectrum of an impact sound:** For a 0.914 mm (diameter). drop at 10 degrees incidence angle.

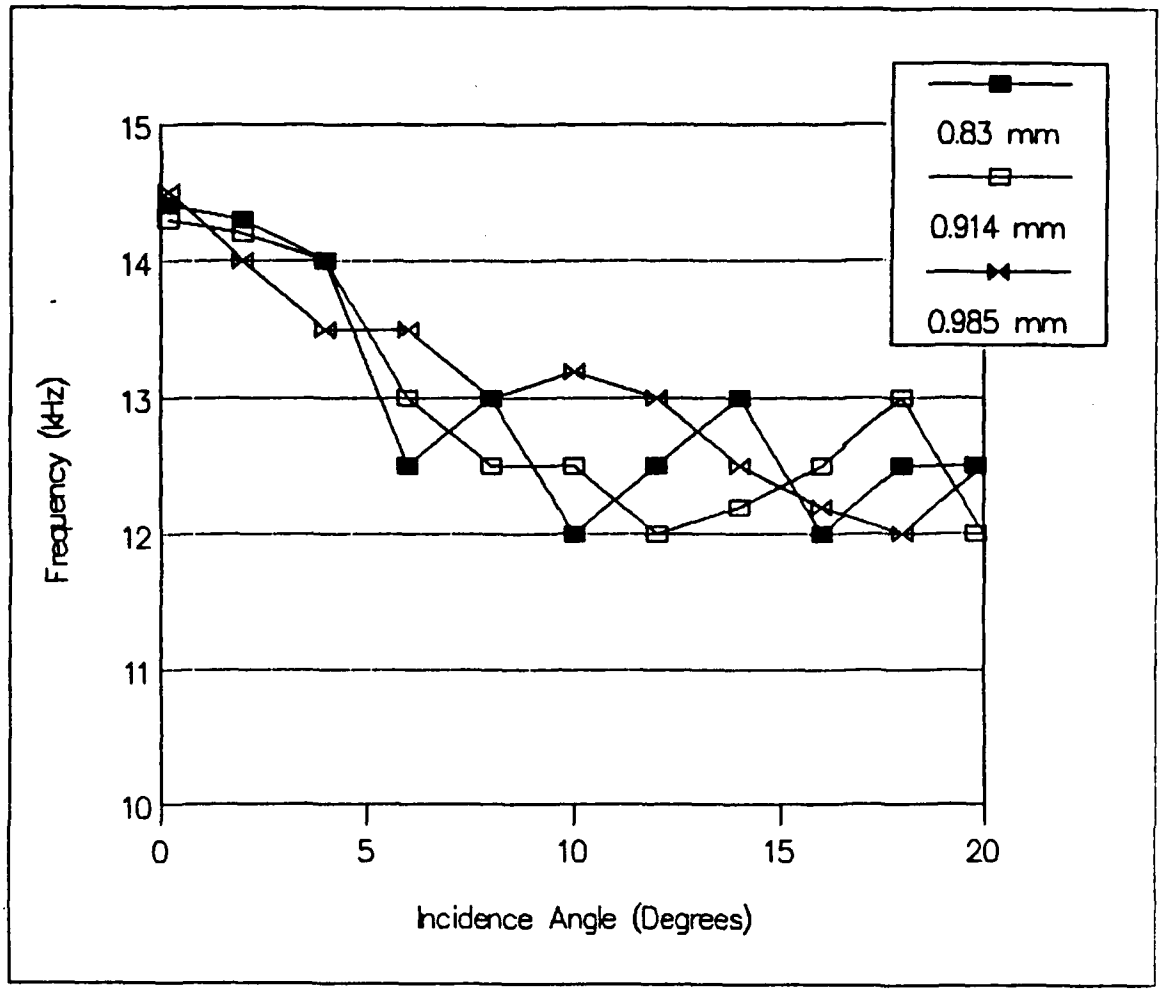


Figure 33. Avg. peak frequencies of impact sound for oblique inc. drops

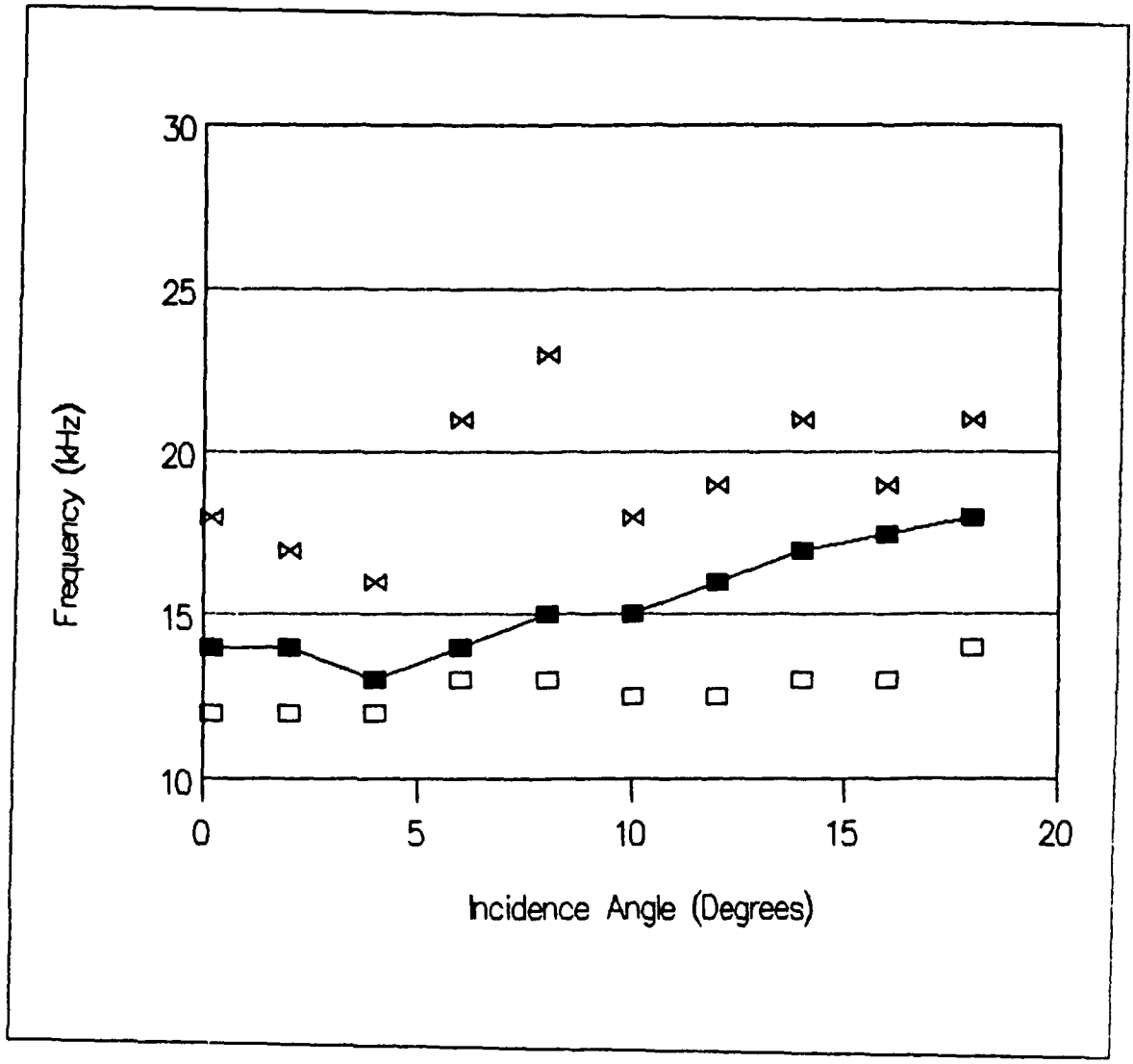


Figure 34. Max. min. and avg. resonance frequencies of bubbles for 0.83 mm drops

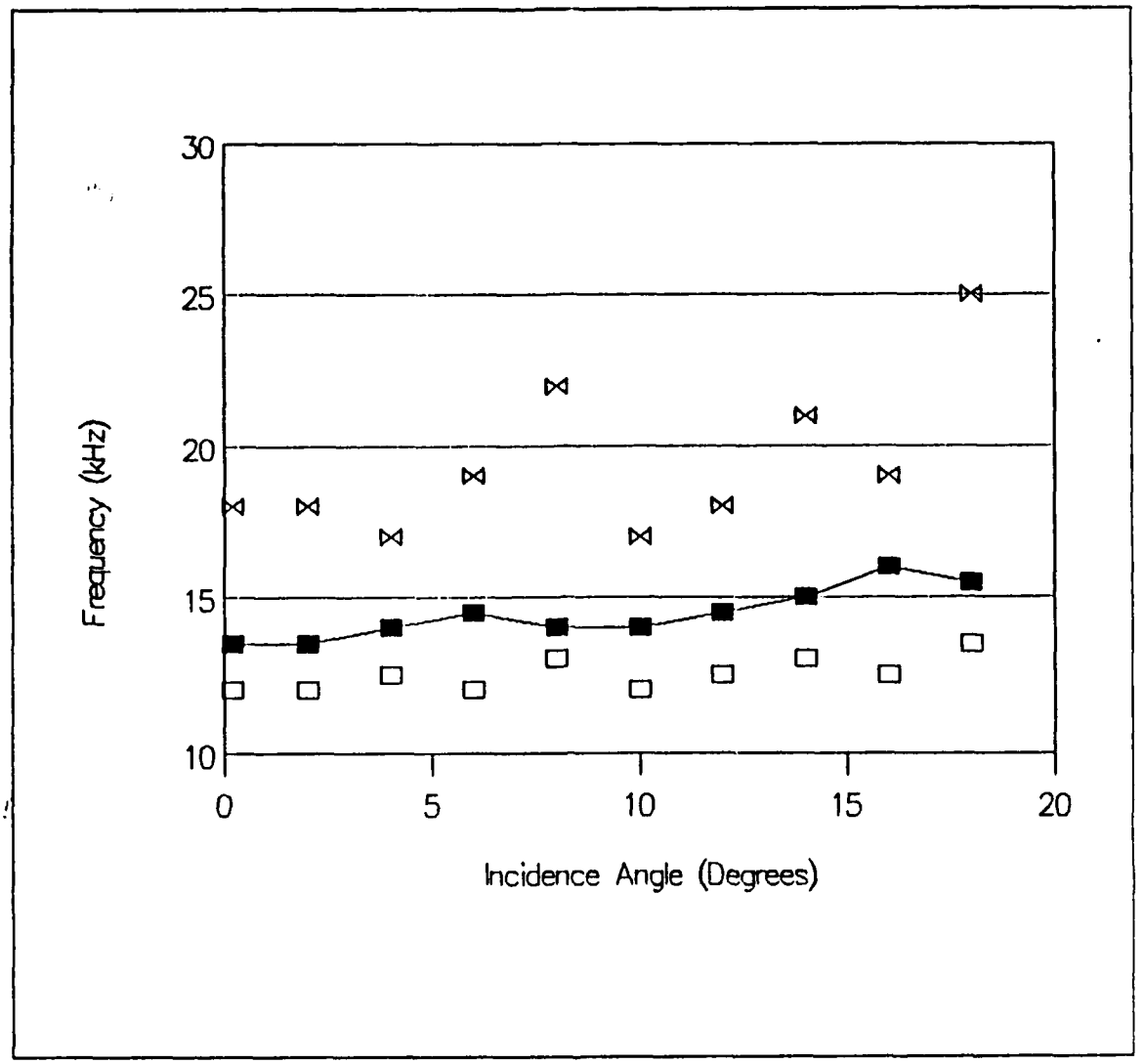


**Figure 35. Max. min. and avg. resonance frequencies of bubbles for 0.914 mm drops**

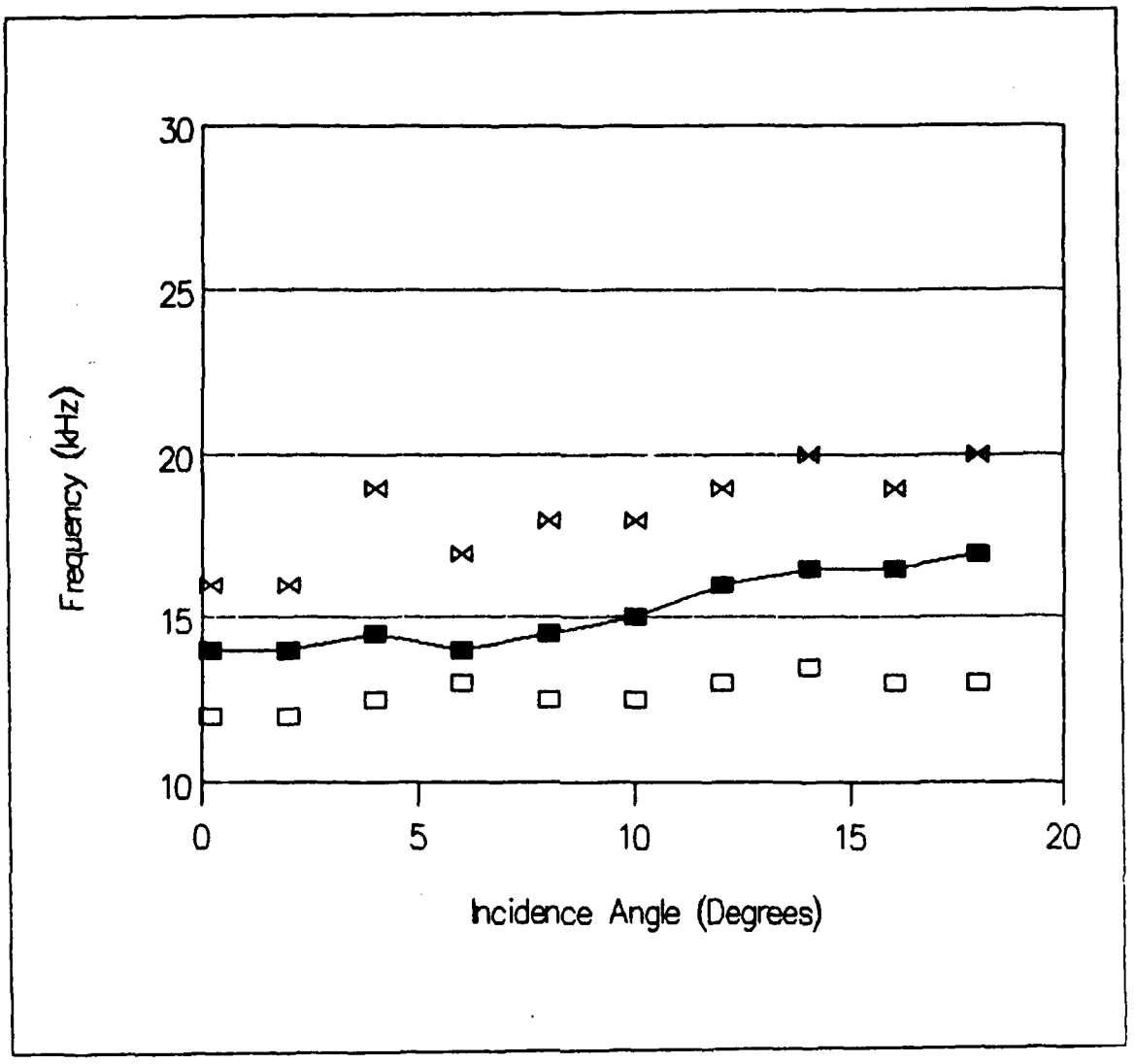


**Figure 36.** Max. min. and avg. resonance frequencies of bubbles for 0.985 mm drops

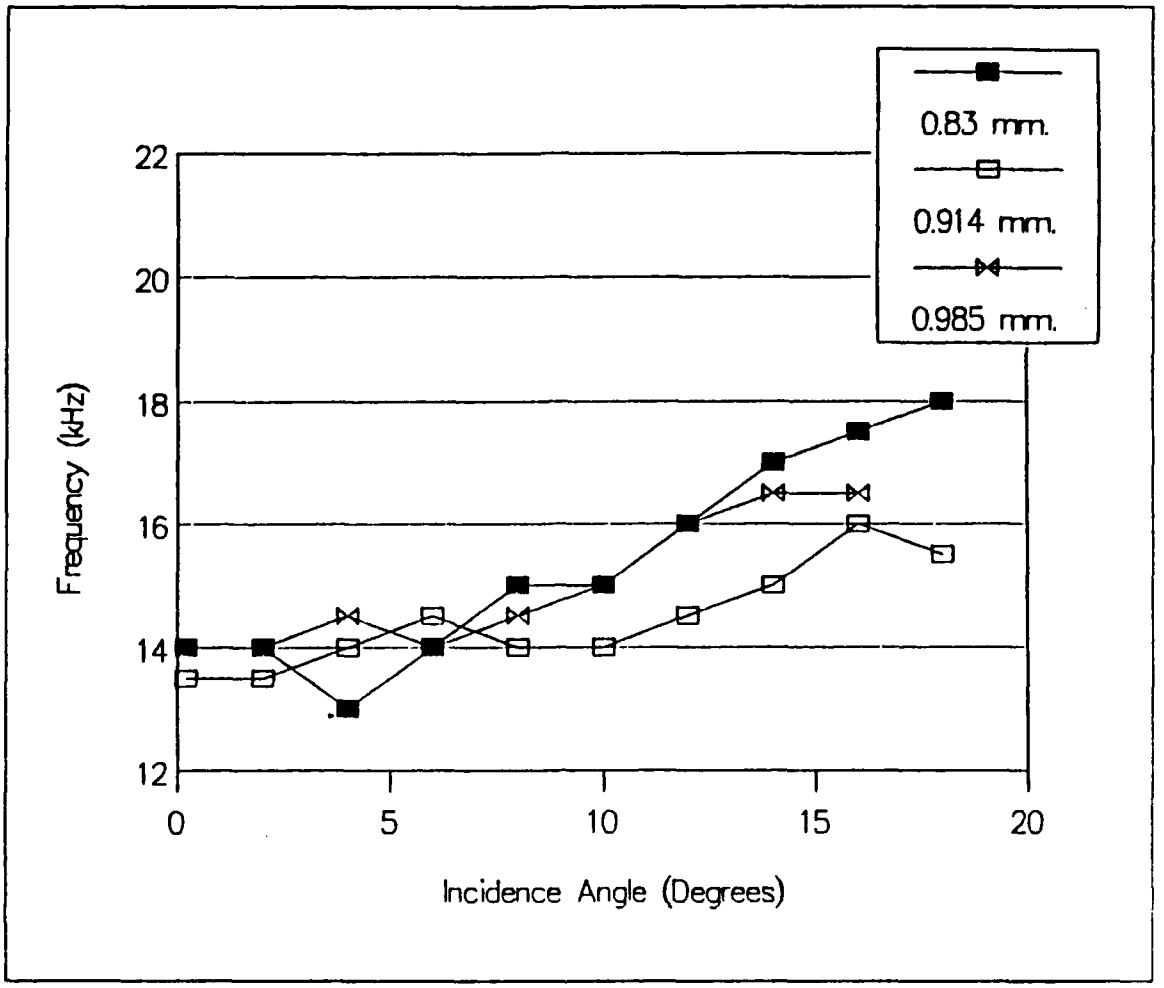


Figure 37. Avg. resonance frequencies of bubbles for oblique incidence drops

### 4. Percentage of Drops Creating Bubbles

The percentage of drops that create bubbles decreases sharply with increasing incidence angle.This is shown in Figure 38. Because bubble creation percentage decreases with increasing angle, the ratio of the average bubble energy to the impact energy decreases sharply as well, with increasing incidence angle. The ratio of the average bubble energy to the impact energy is as shown in Figure 39.

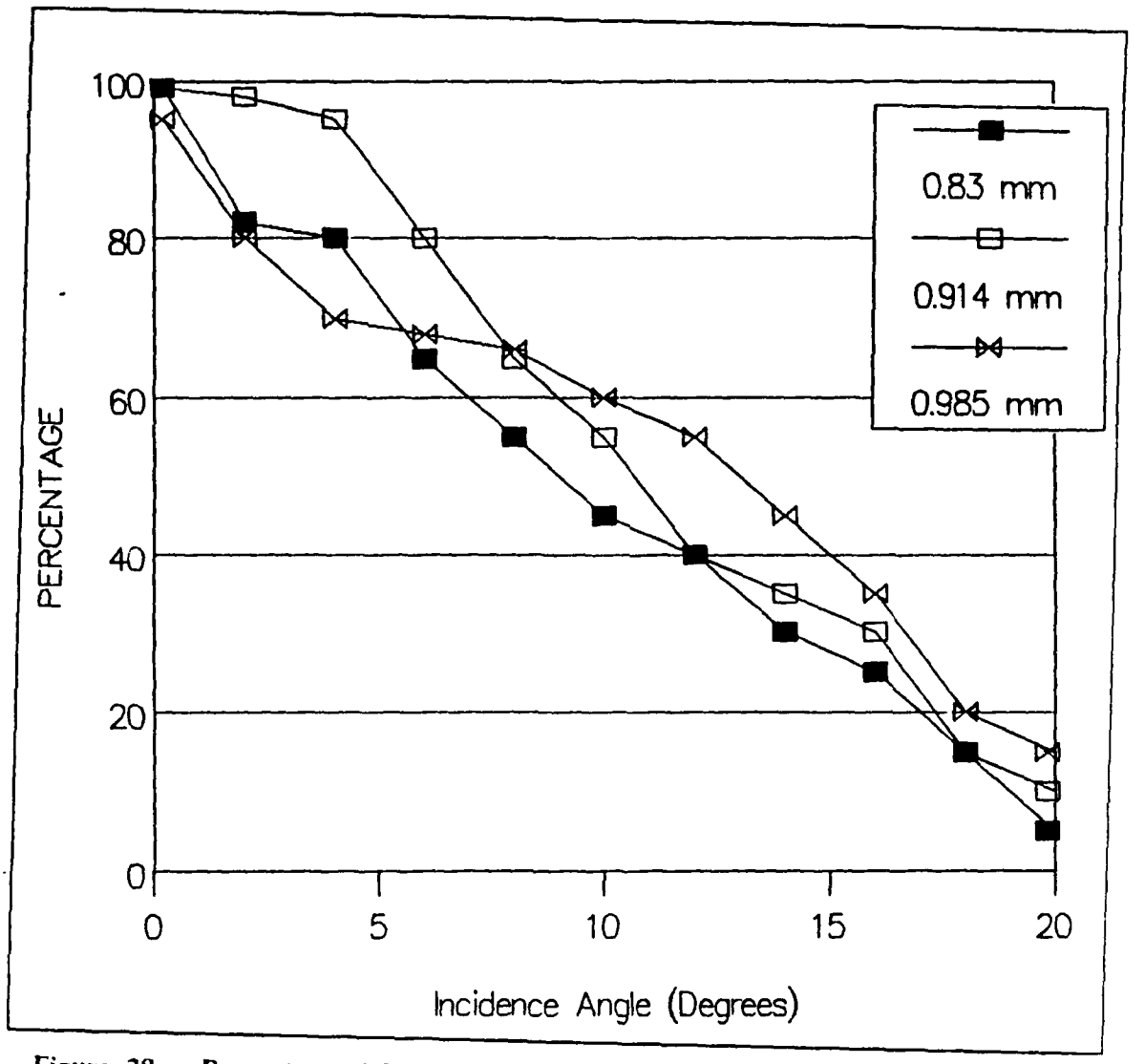


**Figure 38. Percentage of drops that create bubbles**

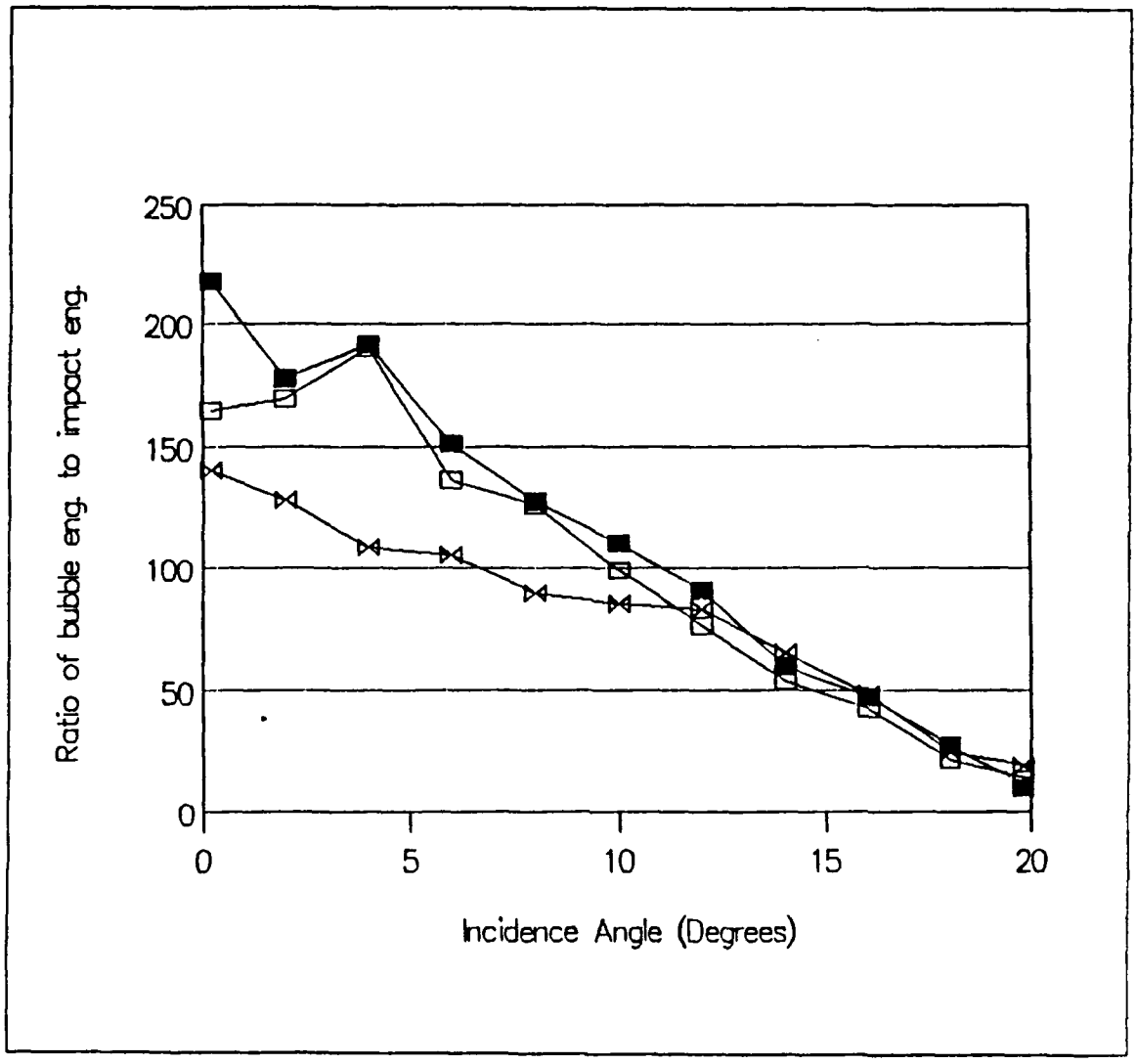


**Figure 39. The ratio of the average bubble energy to the impact energy:** The sharp decrease in the ratio of the bubble enery to the impact energy is mostly due to the sharp decrease in the percentage of the drops that create bubbles with increasing incidence angle.

### 5. Radiation Pattern

To determine the radiation pattern of the impact and of the bubble sound the 8 hydrophone array shown in Figure 19 was used with the hydrophones placed every 20 degrees on each side of the vertical axis with a highly sensitive hydrophone on the center as in the normal incidence case. The polar radiation patterns of bubbles for different sizes of drops and for different incidence angles are as shown in Figures 40 and 41.

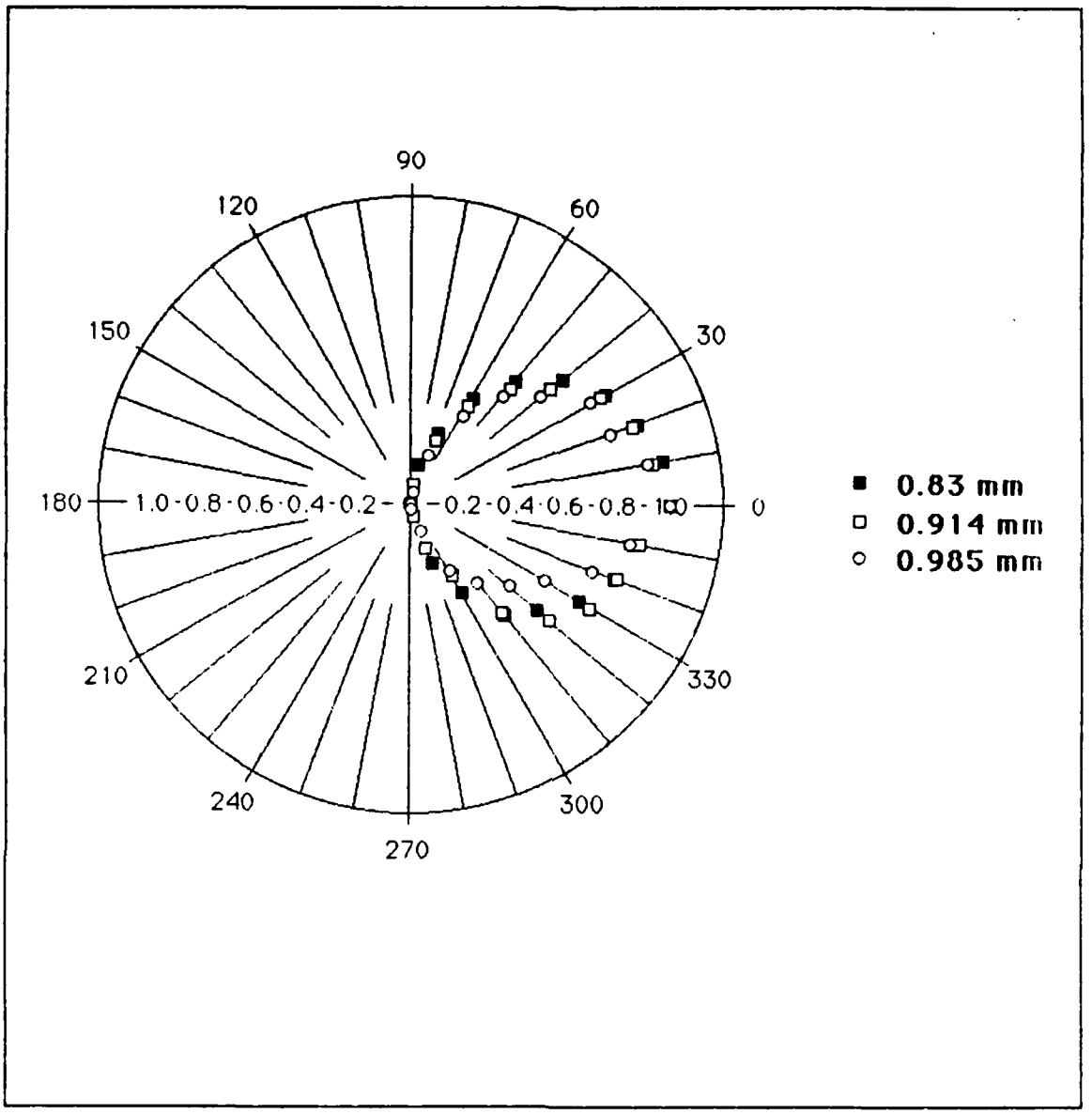


**Figure 40. Polar radiation pattern of bubbles for 10 degrees incidence:** Radiation pattern of 0.83 mm, 0.914 mm and 0.985 mm diameter drops for 10 degrees incidence

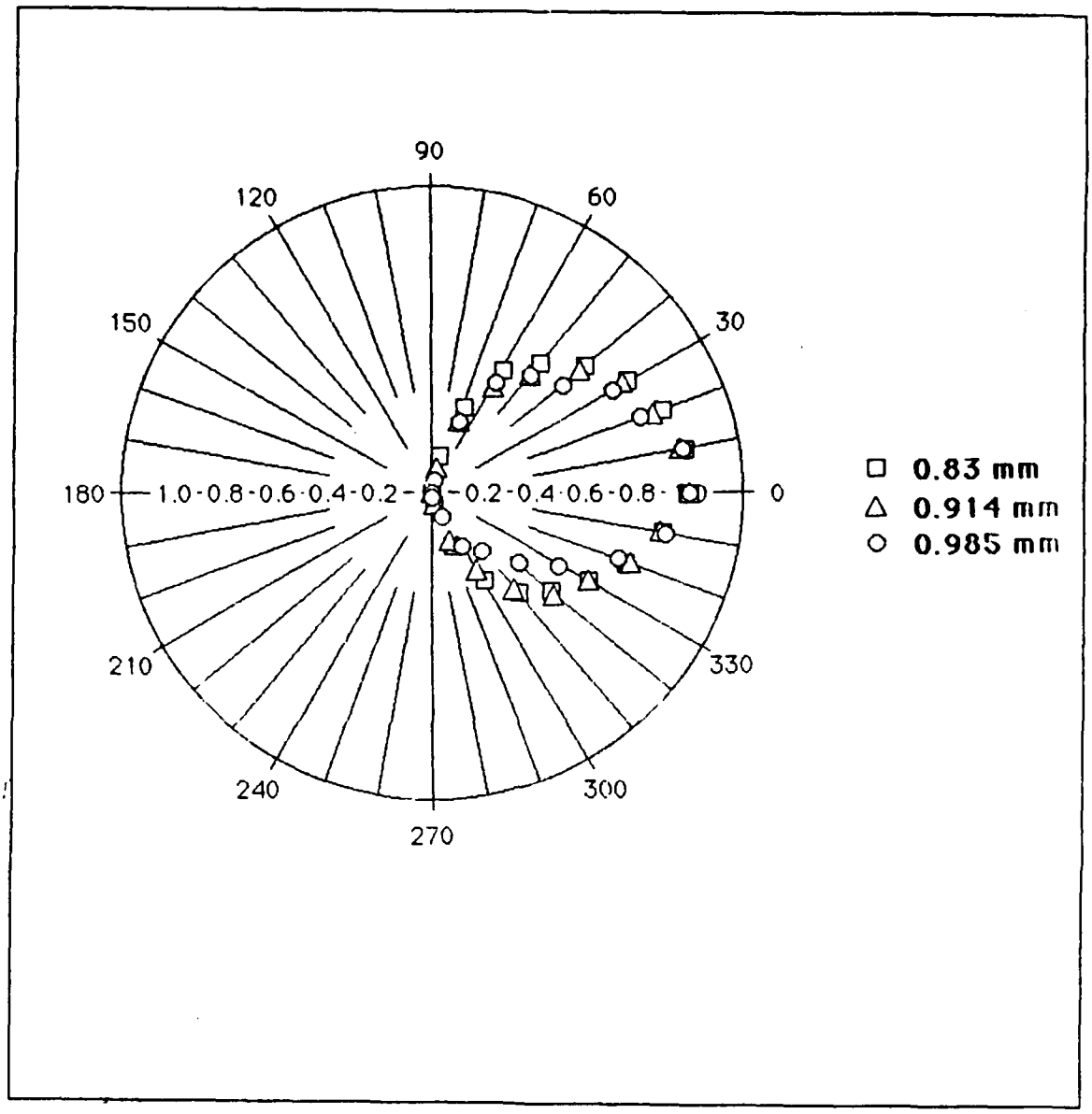


**Figure 41. Polar radiation pattern of bubbles for 20 degrees incidence:** Radiation pattern of 0.83 mm, 0.914 mm and 0.985 mm diameter drops for 20 degrees incidence

# IV. CONCLUSIONS

There have been several theoretical studies and laboratory experiments to understand rain noise at the sea. Previous experimental studies have considered only normal incidence drops, often at less than terminal velocities.They have concentrated on either bubble noise (Crum and Pumphrey) or impact noise (Franz, Nystuen). All the theoretical studies have also considered only normal incidence (Longuet-Higgins, Prosperetti, Nystuen). But rainfall consists of oblique incidence as well as normal incidence drops. For this reason we have studied both normal and oblique incidence drops. We have observed several new and interesting results as well as verified several previous experimental results.

We can conclude that for both normal and oblique incidence, if a bubble is created, the individual bubble has more energy than the individual impact and the total acoustic energy (bubble plus impact) of underwater sound generated by raindrops is much less than the kinetic energy of the drops.

For normal incidence, bubble noise increases with decreasing drop size. On the contrary, impact noise increases with increasing drop size. Both impacts and bubbles have spectral peaks around 15 kHz. The radiation pattern for bubble noise is very close to dipole.

For oblique incidence, the impact energy increases with both increasing drop size and increasing incidence angle. When bubbles are formed, the energy per bubble does not change significantly with changing incidence angle but increases with decreasing drop size (as in the normal incidence case) for all angles.

The percentage of drops creating bubbles decreases sharply with increasing incidence angle. At 20 degrees of incidence, which corresponds to wind speed of 1.3 $\frac{m}{s}$, less then 5 % of the drops create bubbles for the three different drop sizes that we have studied. Considering this sharp decrease in the percentage of drops creating bubbles, we can conclude that the average acoustic energy radiated by the bubbles decreases significantly with increasing incidence angle. This explains the reduction in the magnitude of the spectral peak observed in natural rainfall with increasing incidence angle, in other words with increasing wind speed. The average resonance frequencies of bubbles increase for oblique incidence. On the other hand the impact spectral peak shifts slightly to lower

frequencies. These factors explain the broadening and shifting of the spectral peak observed in natural rainfall with increasing wind speed.

# APPENDIX A. PREAMPLIFIER 1

The block diagram of the preamplifier to obtain a flat 58 dB amplification between 5 kHz and 45 kHz.

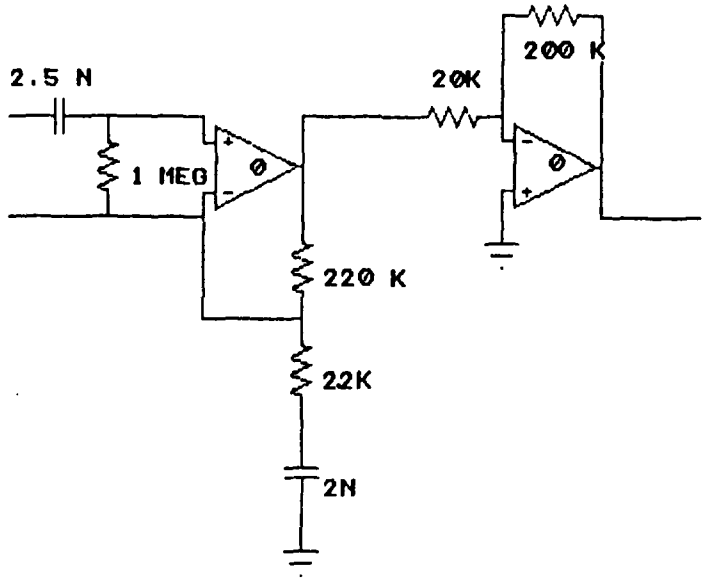

# APPENDIX B. PREAMPLIFIER 2

The block diagram of the second type, simpler preamplifier to obtain a flat 55 dB amplification between 5 and 45 kHz.

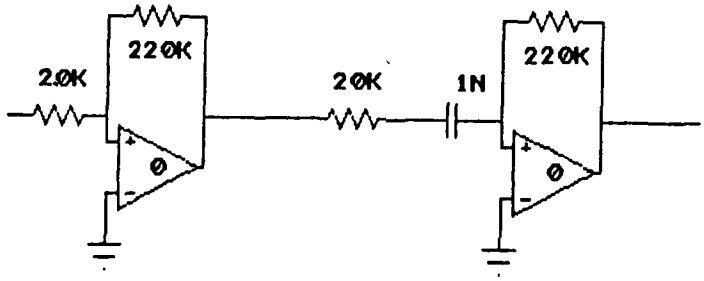

## LIST OF REFERENCES


Longuet-Higgins, M. S. , 1989 : An analytic model of sound production by rain-drops, *Journal of Fluid Mechanics* (Submitted for publication, June 1989)

Franz, G. J. , 1959 : Splashes as sources of sound in liquids, *Journal of the Acoustical Society of America* 31, 1080-1096

Oguz, H. N. and Prosperetti, A. , 1989 : Bubble entrainment by the impact of drops on liquid surfaces, (preprint, May 1989)

Nystuen, J. A. and Farmer, D. M. , 1987 : The influence of wind on the underwater sound generated by light rain, *Journal of the Acoustical Society of America* 82, 270-274

Pumphrey, H. C. and Crum, L. A. , 1989 : Sources of ambient noise in the ocean : an experimental investigation, *Technical Report prepared for Office of Naval Research* May 1989

Wang, P. K. and Pruppacher, H. R. , 1977 : Acceleration to Terminal Velocity of Cloud and Raindrops *Journal of the Acoustical Society of America* 16, 275-280

Medwin, H. and Beaky, M. M. , 1989 : Bubble Sources of the Knudsen Sea Noise Spectra *Journal of the Acoustical Society of America* 86(3), 1124-1130

## INITIAL DISTRIBUTION LIST

| | | No. Copies |
|---|---|---|
| 1. | Defense Technical Information Center<br>Cameron Station<br>Alexandria, VA 22304-6145 | 2 |
| 2. | Library, Code 0142<br>Naval Postgraduate School<br>Monterey, CA 93943-5002 | 2 |
| 3. | Department of Physics<br>Attn: Professor H. Medwin, Code 61Md<br>Naval Postgraduate School<br>Monterey, CA 93943 | 6 |
| 4. | Department of Physics<br>Attn: Professor A. A. Atchley<br>Naval Postgraduate School<br>Monterey, CA 93943 | 2 |
| 5. | Department of Oceanography<br>Attn: Professor J. A. Nystuen<br>Naval Postgraduate School<br>Monterey, CA 93943 | 2 |
| 6. | Dz. Kd. Utgm. Armagan Kurgan<br>4. cadde No : 152 12 (06510)<br>Emek Mahallesi-Ankara / TURKEY | 3 |
| 7. | Deniz Kuvvetleri Komutanligi<br>Personel Daire Baskanligi<br>Bakanliklar-Ankara / TURKEY | 1 |
| 8. | Seyir Hidrografi ve Osinografi Daire Baskanligi<br>Cubuklu - Istanbul / TURKEY | 2 |

9. Deniz Harp Okulu Komutanligi — 2
Tuzla - Istanbul / TURKEY

10. Ortadogu Teknik Universitesi — 1
Cevre Bilimleri
Ankara TURKEY

11. Istanbul Teknik Universitesi — 1
Cevre Bilimleri
Istanbul TURKEY

12. Dokuz Eylul Universitesi — 1
Cevre Bilimleri
Izmir / TURKEY

13. Commanding Officer — 1
Naval Environmental Prediction Research Facility
Monterey, CA 93943

14. Dr. Marshall Orr — 1
Office of Naval Research (Code 11250A)
800 N. Quincy Street
Arlington, VA 22217

15. Prof. L. A. Crum — 1
The National Center for Physical Acoustic
University, MS 38677

16. Prof. M. S. Longuet-Higgins — 1
Center for Studies of Nonlinear Dynamics
La Jolla Institute
7855 Fay Avenue, Suite 320
La Jolla, CA 92037

17. Dz.Kd.Utgm Rusen Olmez — 1
Dostlar Sitesi, C Blok, No: 111
Balgat-Ankara Turkey

18. Dr David Farmer — 1
Institute of Ocean Sciences
P.O. Box 6000, Sydney B.C.
V8L 4B2 , Canada